THE ASIAN WINTER - AUSTRALIAN SUMMER MONSOON: AN INTRODUCTION

C.-P. CHANG

Department of Meteorology
Graduate School of Engineering and Applied Sciences
Naval Postgraduate School, Monterey, California, USA
E-mail: cpchang@nps.edu

During boreal winter, the maximum heating moves from its boreal summer location over South Asia in to the Maritime Continent – northern Australian region. North of the equator, low-level northeasterly winds prevail over a large longitudinal span, from the western Pacific to Indian Ocean. Although differential heating and the resultant thermal direct circulation are responsible for both the Asian winter and the Asian summer monsoon circulations, but the two monsoons differ in more than one way. On the one hand, the heat source region of the Asian winter monsoon is much closer to the equator (Krishnamurti 1971); but on the other hand, the circulation of the Asian winter monsoon encompasses a larger meridional domain such that the tropical region has a strong interaction with the extratropical region (Boyle and Chen 1978, Chan and Li 2004). As a result, baroclinic development in middle and high latitudes usually has a stronger influence on equatorial regions in the Asian winter monsoon than the Asian summer monsoon.

The region "Maritime Continent" was defined by Ramage (1968) to consist of Malaysia, Indonesia, and the surrounding land and oceanic areas of the equatorial western Pacific between 10°S - 10°N. This is a region of strong seasonal reversal of winds that is often coupled with the annual variation of rainfall, particularly near the equator where the prevailing wind is westerly during the wet season of boreal winter and easterly during the dry season of boreal summer (e.g., Ramage 1971; Masumoto 1992; McBride 1998; Hamada *et al.* 2002; Chang *et al.* 2004). The rainfall variation in this region is in phase with that of the northern Australia monsoon (McBride 1987, 1998; Hendon and Liebmann, 1990a). Therefore, the terms Asian winter monsoon, northern winter monsoon or Australian (summer) monsoon are sometimes used to include the wet monsoon in both regions. The latent heat release over the combined Maritime Continent – northern Australia area is one of two major heat sources of the boreal winter atmosphere. This has long been recognized as a major planetary-scale heat source that provides a significant amount of the energy that drives the global circulation during boreal winter.

The interaction of this heat source with strong East Asian baroclinic system and cold air outbreaks may affect the East Asian jet (Chang and Lau 1982, Lau and Chang 1987) and in turn influence the weather in North America (Yang *et al.* 2002). Recent analysis also suggest that flare-ups of this Maritime Continent heat source may lead to downstream wave-train propagation and may be related to storm development over Europe ten days later (Thorpe *et al.* 2002). In a general circulation model study, Neale and Slingo (2003) demonstrated that the tendency of a dry bias in the Maritime Continent region is a major source for systematic errors over both tropical Indian and Pacific oceans and extratropical North America and Northeast Europe. They concluded that the Maritime Continent plays a critical role in the global circulation and emphasized the need for better representation of

convective organization over this region of complex land–sea terrains.

The Asian winter monsoon season also coincides with the period of the highest tropical cyclone activities of the southwestern Pacific (Holland 1984, McBride 1995). The monsoon trough south of the equator is a favorable area of tropical cyclone development during boreal winter, particularly under the influence of the Madden-Julian Oscillation (Madden and Julian 1972, Hendon, and Liebmann, 1990b, Hendon *et al.* 1999). In addition, the rare equatorial tropical cyclogenesis of Typhoon Vamei, 2001, at 1.5°N near Singapore was a result of interactions of monsoonal cold surges and local circulations (Chang *et al.* 2003). Both the East Asian winter monsoon and the Australian monsoon are also affected directly by ENSO and other interannual and decadal variations in the Pacific and Indian Oceans.

References

Boyle, J. S., and G. T.-J. Chen, 1987: Synoptic aspects of the winter time East Asian monsoon. *Monsoon Meteorology*, C.-P. Chang and T. N. Krishnamurti, Eds., Oxford University Press, 125-160.

Chan, J. C-L, and C. Li, 2004: The East Asian Winter Monsoon. *East Asian Monsoon*, C.-P. Chang, Ed., World Scientific, in press.

Chang, C.-P, and K. M. Lau, 1982: Short-term planetary-scale interactions over the tropics and midlatitude during northern winter. Part I: Contrasts between Active and Inactive Periods. *Mon. Wea. Rev.*, **110**, 933-946.

Chang, C.-P, C. H. Liu, and H. C. Kuo, 2003: Typhoon Vamei: An equatorial tropical cyclone formation. *Geophys. Res. Lett.,* **30**, 50 1-4.

Chang, C.-P, P. A. Harr, and J. McBride, 2004: Maritime Contient Monsoon. *East Asian Monsoon*, C.-P. Chang, Ed., World Scientific, in press.

Hamada, J.-I., M. D. Yamanaka, J. Matsumoto, S. Fukao, P. A. Winarso, and T. Sribimawati, 2002: Spatial and temporal variations of the rainy season over Indonesia and their link to ENSO. *J. Meteor. Soc. Japan*, **80**, 285-310.

Hendon, H.H. and B. Liebmann, 1990a: A composite study of onset of the Australian summer monsoon. *J. Atmos. Sci*., 47, 2227–2240.

Hendon, H.H. and B. Liebmann, 1990b: The intraseasonal (30–50 day) oscillation of the Australian summer monsoon. *J. Atmos. Sci*., 47, 2909–2923.

Hendon, H.H., C. Zhang, and J.D. Glick, 1999: Interannual variation of the Madden-Julian oscillation during Austral Summer. *J. Climate*, 12, 2538–2550.

Krishnamurti, T. N., 1971: Tropical east-west circulations during northern summer. *J. Atmos. Sci*., **28**, 1342-1347.

Holland, G. J., 1984: On the climatology and structure of tropical cyclones in the Australian Southwest Pacific Region. *Aus. Meteor. Mag*., **32**, 17-31.

Lau, K. M., and C.-P. Chang, 1987: Planetary scale aspects of winter monsoon and teleconnections. *Monsoon Meteorology*, C.-P. Chang and T. N. Krishnamurti, Eds., Oxford University Press, 161-202.

Matsumoto, J., 1992: The seasonal changes in Asian and Australian monsoon regions. *J. Meteor. Soc. Japan*, **70**, 257-273.

McBride, J., 1987: The Australian summer monsoon. *Monsoon Meteorology*, C.-P. Chang and T. N. Krishnamurti, Eds., Oxford University Press, 203-231.

McBride, J., 1995: Tropical cyclone formation. *Global Perspective on Tropical Cyclones*, R. L. Elsberry, Ed., Tech. Docu. 693, World Meteorological Organization, 63-105.

McBride, J., 1998: Indonesia, Papua New Guinea, and tropical Australia: The southern hemisphere summer monsoon. *Meteorology of the Southern Hemisphere*, Meteor. Monogr., No. **49**, Amer. Meteor. Soc., 89–99.

Neale, R., and J. Slingo, 2003: The Maritime Continent and its role in the global climate: A GCM Study. *J. Climate,* **16**, 834-848.

Ramage, C. S., 1968: Role of a tropical "Maritime Continent" in the atmospheric circulation. *Mon. Wea. Rev*., **96**, 365-369.

Ramage, C. S., 1971: *Monsoon Meteorology*. Acad. Press, 296pp.

Thorpe, A., M. Shapiro, and R. Langland, 2003: Presentation of THORPex Project to WMO/CAS, February 13, 2002, Oslo. (http://www.mmm.ucar.edu/uswrp/powerpoint/thorpex/v3_document.htm).

Yang, S., K.-M. Lau, and K.-M. Kim, 2002: Variations of the East Asian jet stream and Asian–Pacific–American winter climate anomalies, *J. Climate*, **15**, 306-325.

A REVIEW OF THE EAST ASIA WINTER MONSOON

JOHNNY C L CHAN

Laboratory for Atmospheric Research
Dept. of Physics & Mat. Sci., City University of Hong Kong
Hong Kong, China
E-mail: Johnny.chan@cityu.edu.hk

1. Introduction

The East Asia winter monsoon (EAWM) generally refers to the atmospheric flow over Asia associated with the eastward and southward movement of cold air coming from the Siberian High. In this review, major characteristics of the EAWM will be described. The first, to be discussed in section 2, is the so-called cold-air "surges" that affect most parts of eastern and southern China, as well as the South China Sea (SCS). These surges not only dominate the weather over China and southeast Asia, but also affect convection over the maritime continent (Chang and Lau 1980), the Southern Hemisphere (SH) monsoon (Davidson *et al.* 1983) and the genesis of tropical cyclones in the SH (Love 1985). In addition, they have been linked to the development of the El Niño/Southern Oscillation (ENSO) event (Li 1990a; Xu and Chan 2001). Other than the surges, a significant effect of the EAWM is the explosive development of low-pressure systems over the East China Sea as the cold air moves off the continent and over the warm water. Such development will be discussed in section 3. A documentation of the temporal variations in the strength of the EAWM on time scales from intraseasonal to interannual and interdecadal will be given in section 4, together with their possible linkages with other oscillations in the atmosphere (e.g. ENSO) or atmospheric and oceanographic conditions. Some unresolved issues that need to be addressed in the future are discussed in section 5.

2. Monsoon surges

Many previous studies of the EAWM have focused on the cold-air surges associated with the EAWM and numerous definitions have been made [Boyle and Chen 1987; Ding 1990a, b; Qiu *et al.* 1992; Ding 1994; Wu and Chan 1995 (hereafter WC95); Zhang *et al.* 1997; Compo *et al.* 1999]. While a universal definition or consensus has yet to be reached, a general agreement is that these surges have the most dramatic effects in the tropics, in initiating convection over the maritime continent and in the subsequent feedback to the subtropical jet aloft. Because most studies on the EAWM focus only on surges from the north but WC95 and Wu and Chan (1997a; hereafter WC97) discussed the evolution of two types of EAWM surges: northerly and easterly, some of their results are summarized to illustrate the physical processes involved. It should also be noted that many of the results on the northerly surge discussed in WC95 and WC97 are similar to those from other researchers.

2.1. Northerly Surges

Based on meteorological parameters measured in Hong Kong, WC95 defined the occurrence of a northerly surge (NS) using changes in temperature as well as wind direction and speed. Their

definition highlights the importance of not only the temperature drop and strengthening of the northerly winds, but also the change in wind direction.

The composite time variations of surface meteorological parameters over Hong Kong during an NS show a sharp rise of ~3 hPa on day 1 relative to day 0 (Fig. 1a), which is consistent with the strengthening of the northerly wind component to ~ 30 km h^{-1} (Fig. 1b) and the temperature drop of ~4°C (Fig. 1c). Note also the decrease in the surface moisture content from the variation in dew-point depression (Fig. 1c) and the significant weakening of the easterly component (Fig. 1b), features that are often not emphasized in most other studies.

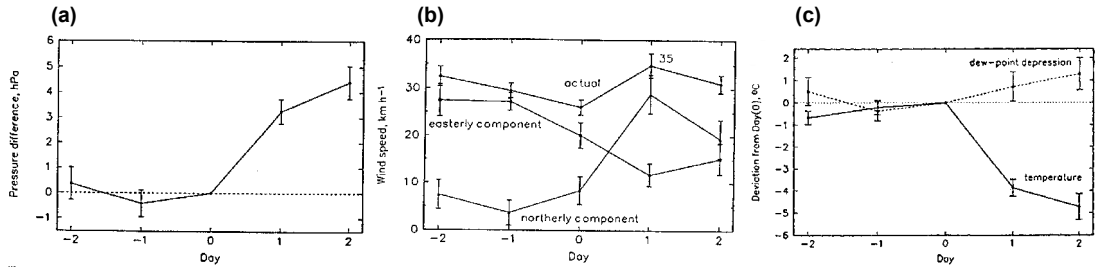

Fig. 1. Composite variations of surface meteorological parameters measured in Hong Kong during the passage of northerly surges from two days before (day –2) to two days after (day 2). Day 0 is the day the NS arrives at Hong Kong. (a) Deviation of mean-sea-level pressure from day 0, (b) actual, easterly and northerly components of the surface wind, and (c) surface temperature (solid) and dew-point depression (dashed) relative to day 0. The vertical bars in all diagrams indicate the standard errors of the data within the sample. (Adapted from WC95)

The composited station data over Asia for the NS cases identified in WC95 show an increase in pressure gradient over the Siberia-Mongolia (SM) region, reaching over 1045 hPa on day (-1) (Fig. 2b). Although the centre of the SM high (SMH) does not exhibit substantial movement, a dramatic equatorward shift in isobars over mainland China can be seen (cf. Fig. 2a with other panels in Fig. 2). The 1026-hPa isobar migrates from northern China (~40°N) on day –2 southward to reach a latitude of ~25°N by day 1 (Fig. 2d), which gives a southward speed of ~ 7 m s^{-1}, a value roughly consistent with the estimate by Chang *et al.* (1983) for their second stage of the surge, the first stage being a gravity-wave type propagation (to be discussed below). Associated with this pressure surge is the surge of cold air, which leads to significant temperature drops over the region (see WC95). Cross-isobaric flow of the surface wind can also be identified (not shown). In addition, the composite surface pressure shown in Fig. 2 at the centre of the SMH is ~1045 hPa. However, for individual cases, a surface pressure as high as 1085 hPa has been reported (Zhao and Ding 1991) and values of > 1050 hPa are not uncommon (Zhang *et al.* 1997; Zhang and Chen 1999). The evolution and dynamics of the SMH will be explored later.

Based on previous observational studies of the EAWM, Lim and Chang (1981) performed a theoretical study on the nature of the NS and suggested that the pressure surge could represent a transient, gravity-wave like motion due to a pressure-wind imbalance, which then allows a fast propagation of energy from the midlatitudes to the tropics. An example of this propagation is given in Fig. 3. Here, two stages of the surge are identified, the first one being a pressure rise (called the "edge") and the second one a significant drop in dew point (the "front"). Chang *et al.* (1983) estimated that the edge (pressure surge) travels at a speed of ~ 40 m s^{-1}, which is much faster than the advective speed (generally ~ 10 m s^{-1}) and is therefore suggestive of a gravity-wave like character. The same NS also produced a drop in dew point but the speed of the front was only ~ 10 m s^{-1}. More recent studies by Chen and Huang (1989) and Zhou (1989) that included ship reports over the SCS further confirmed the gravity-wave characteristics of the pressure surge over the SCS.

The geopotential height distributions at 1000 hPa are rather similar to those at the surface, with

the center of the SMH anchored to the southwest of Lake Baikal (Fig. 4a). The average height value at the center increases from ~280 m at day –1 to ~310 m at day 0 (not shown). The cold pocket that moves out of the SMH can best be seen at 850 hPa (Fig. 4b) where a southeastward trajectory is apparent, which is consistent with the result of Ding and Krishnamurti (1987) and Zhang *et al.* (1997). The location of the 1000-500 hPa minimum thickness shown in Fig. 4b also suggests that the lower tropospheric air mass migrates eastward, which follows a trough passage at 500 hPa (see below). Such a vertical tilt is consistent with the development of a baroclinic wave (Holton 1992).

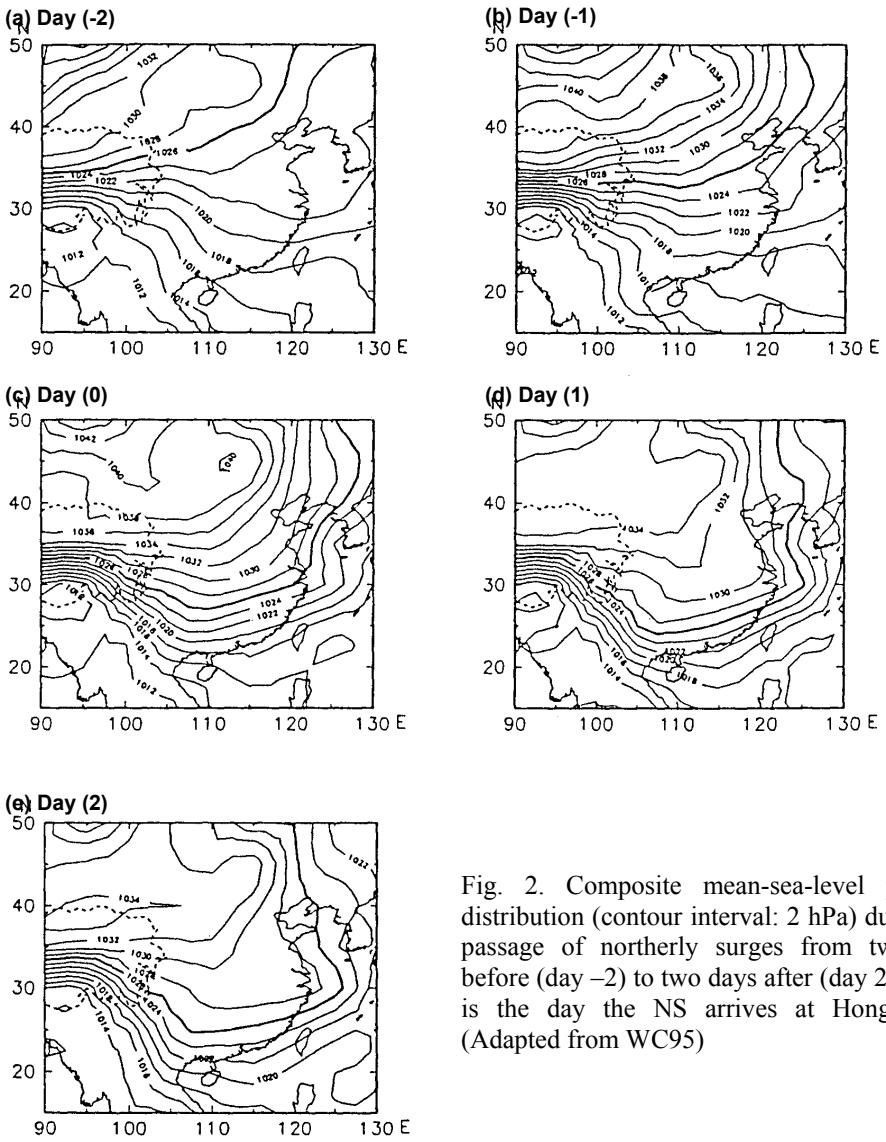

Fig. 2. Composite mean-sea-level pressure distribution (contour interval: 2 hPa) during the passage of northerly surges from two days before (day –2) to two days after (day 2). Day 0 is the day the NS arrives at Hong Kong. (Adapted from WC95)

The propagation of the jet stream is best identified from the zonal wind variations at 500 hPa (Fig. 5). At day –3, zonal winds over the Tarim Basin strengthen, which corresponds to the passage of the polar jet from upstream near Lake Balkhash (45°N, 75°E) (not shown). This jet streak propagates eastward and then merges with the subtropical jet by day –1 (Fig. 5a) to form the East Asian jet that continues to migrate eastward to Japan by day 0 and day 1 (Figs. 5b and c). The jet further strengthens on day 2 and day 3 due to a return flow from the equatorial region [not shown; see Chang and Lau (1980); Ding and Xiao (1992) or WC97 for a discussion of this feature], which is basically an enhancement of the Hadley cell leading to northward transport of angular momentum so that the subtropical jet or East Asian jet, is strengthened (see also Palmén and Newton 1969).

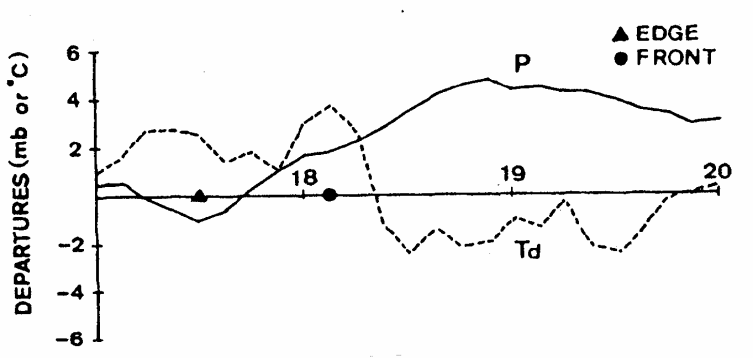

Fig. 3. Example of how the edge and front times of a surge are defined based on the time series of pressure (solid) and dew point (dashed) at Taipei. The departures are from seasonal averages. (from Chang *et al.* 1983)

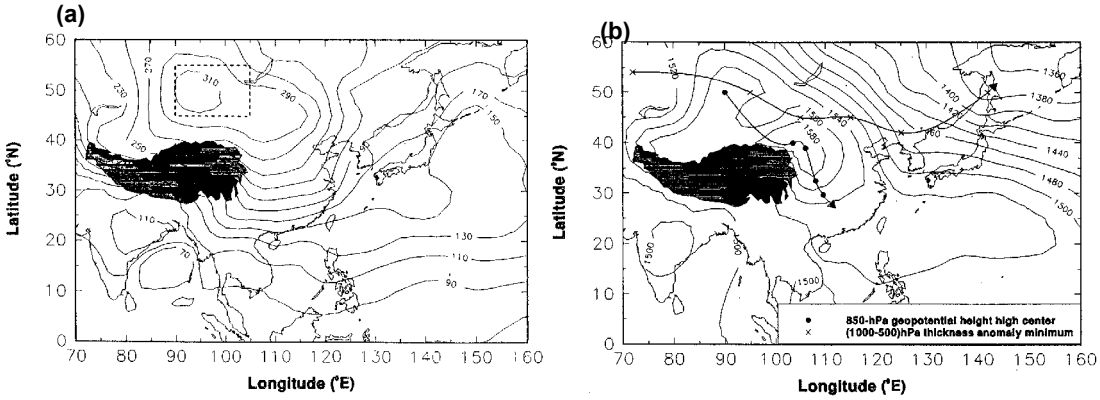

Fig. 4. Composite geopotential height (gpm) at (a) 1000 hPa and (b) 850 hPa of an NS on day 0. In (a), the dashed box defines the region of the SMH. In (b), the solid curves indicate the track of the (local) maximum 850-hPa height center from 1200 UTC on day –1 to 1200 UTC on day 1 (bottom track, dots every 12 h) and the 1000–500 hPa (local) minimum thickness anomaly from day –3 to day 2 (top track, crosses every 12 h). Blackened area indicates the Tibetan Plateau with altitude greater than 3 km. (Adapted from WC97)

Since the NS originates from the SMH, it is of interest to examine the synoptic-scale features associated with this high-pressure system. The passage of an upper-level shortwave trough over the SMH (45-55°N, 90-105°E, region marked in Fig. 4a) is obvious from the time-pressure cross-section of relative vorticity (Fig. 6a) and geopotential height (Fig. 6b) averaged over the SMH domain. Strong cyclonic vorticity is observed at 300 hPa at around day –2 to day –1 (Fig. 6a) while the decrease in geopotential height appears to occur a little earlier (Fig. 6b). Below ~ 700 hPa, the geopotential height anomaly increases from ~day -1, which is accompanied by strong divergence (Fig. 6c). The increase in geopotential height anomaly and positive divergence suggests that the SMH is intensifying. Prior to this, the level of maximum divergence is actually at the upper levels, with weak convergence at the low levels. This implies that between days –3 and –4, strong rising motion occurs in the mid troposphere. This can also be inferred by examining the vertical distribution of absolute vorticity advection (Fig. 6d). During this time, absolute vorticity advection increases with height in the mid to upper troposphere. A similar pattern is observed in the potential temperature advection variations (not shown – see WC97). Then, as the shortwave trough passes, the vertical variation of vorticity advection reverses sign, which implies sinking motion. Notice that near day –1 and day 0, while the strongest vertical gradient of vorticity gradient is in the mid troposphere, the divergence extends all

the way up to the upper troposphere (Fig. 6c). This means that the sinking motion does not result from the passage of the upper-level shortwave. Rather, it is induced by the strong divergence near the surface. Then at day 1, the anticyclone upstream of the shortwave (Fig. 6a) leads to an increase in geopotential height (Fig. 6b), which forces convergence through a deep layer (Fig. 6c) and a subsequent warming (not shown) and the weakening of the cold pool.

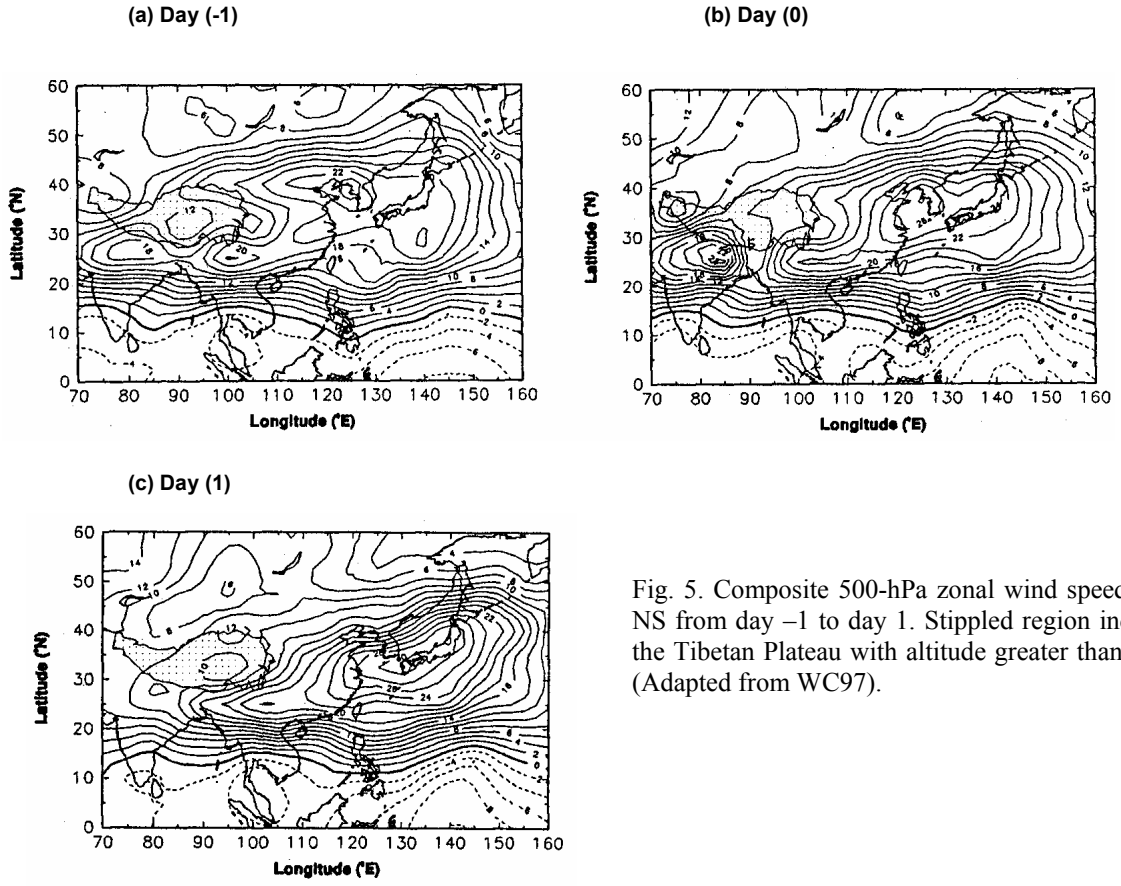

Fig. 5. Composite 500-hPa zonal wind speed of an NS from day –1 to day 1. Stippled region indicates the Tibetan Plateau with altitude greater than 3 km. (Adapted from WC97).

Based on the local and synoptic-scale features described above, the physical processes involved in the evolution of an NS may be as follows. The initiation of the NS begins with the eastward passage of a polar jet streak west of Lake Balkhash. As the jet streak passes over the SMH domain, the thermally indirect transverse circulation at the exit region of the jet, coupled with the circulation ahead of the trough in a developing baroclinic wave, forces strong rising motion over the SMH, which leads to strong cooling and an intensification of the SMH (Fig. 7a). With the continued eastward propagation of the jet streak, the SMH domain is then in the entrance region of the jet so that subsidence now occurs over the main part of the domain, which is enhanced by the anticyclonic advection to the backside of the baroclinic trough (Fig. 7b). The sinking motion therefore builds up the SMH to its maximum intensity. An outpour of the cold air in the lower troposphere then occurs, which leads to further upper-level convergence and sinking motion. As this cold dome pushes southward, the polar jet also migrates in tandem and merges with the subtropical jet stream to form the East Asian jet. The subsidence warming eventually over-compensates radiational cooling, and leads to warming of the column. Together with the discharge of the cold air, the SMH then weakens. In the lower troposphere, the southward push of the cold air then excites gravity waves that propagate across the SCS. Convection breaks out over the maritime continent and the northward outflow from the deep convection then causes a second strengthening of the East Asian jet in the vicinity of Japan. This then completes the cycle of an NS.

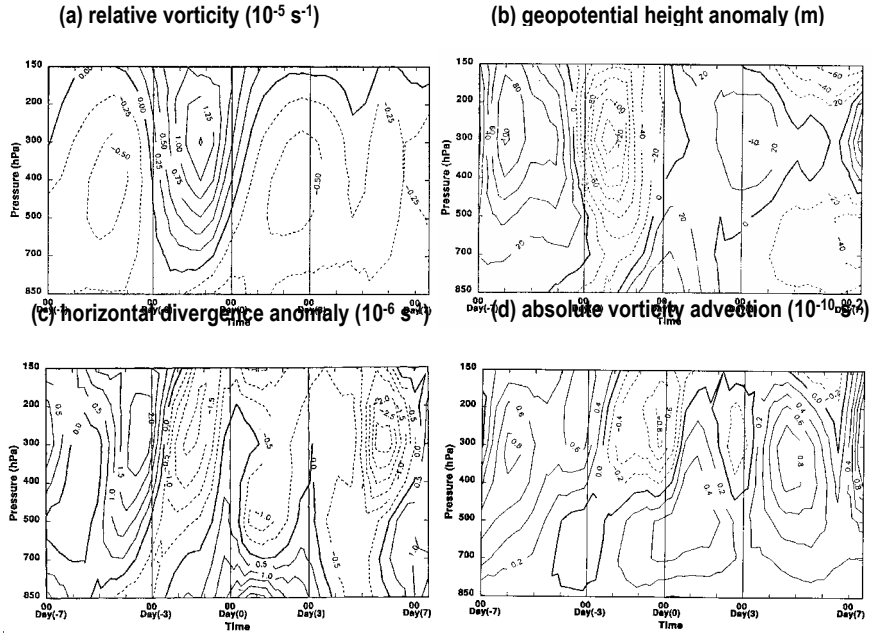

Fig. 6. Time variations over the SMH region of (a) relative vorticity, (b) geopotential height anomaly, (c) horizontal divergence anomaly, and (d) absolute vorticity advection associated with an NS from day –7 to day 7. (Adapted from WC97)

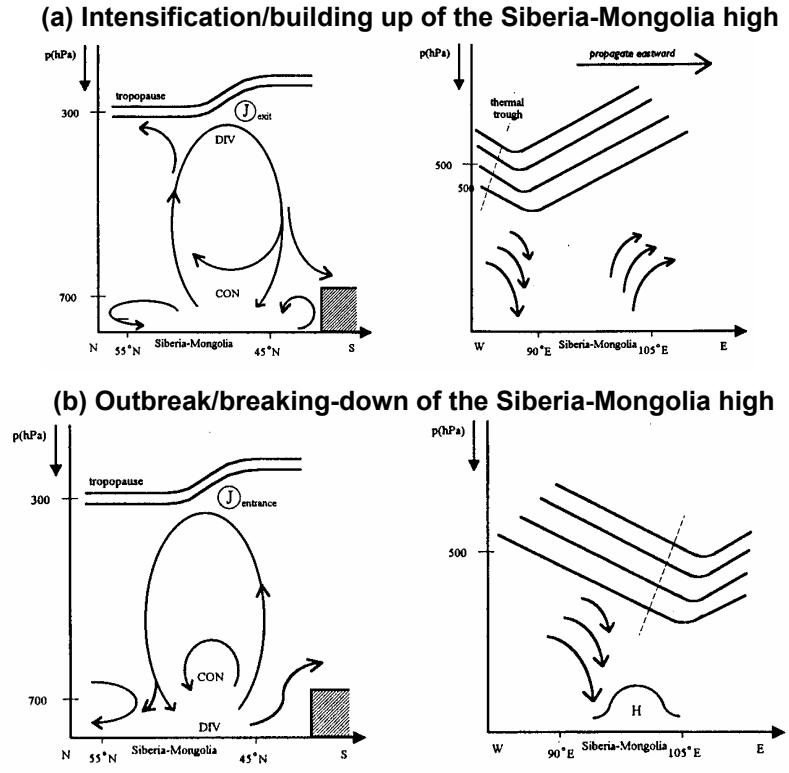

Fig. 7. Schematic showing the evolution of the SMH in an NS at the stages of (a) intensification, and (b) outbreak. Left panels show the transverse circulation associated with the jet (marked with J and circled) and the (a) exit and (b) entrance regions. Right panels show the secondary circulation associated with the passage of the height and thermal trough when (a) the shortwave is heading toward, and (b) away from the SMH region. (Adapted from WC97)

2.2. Easterly Surges

As discussed in the Introduction, the easterly surge (ES) is generally not discussed in most of the literature on the EAWM because relative to the NS, its main effect appears to be primarily in the strengthening of the winds and is quite localized. However, the ES represents a type of surge that is also initiated as a result of the movement of a cold dome and is therefore part of the EAWM.

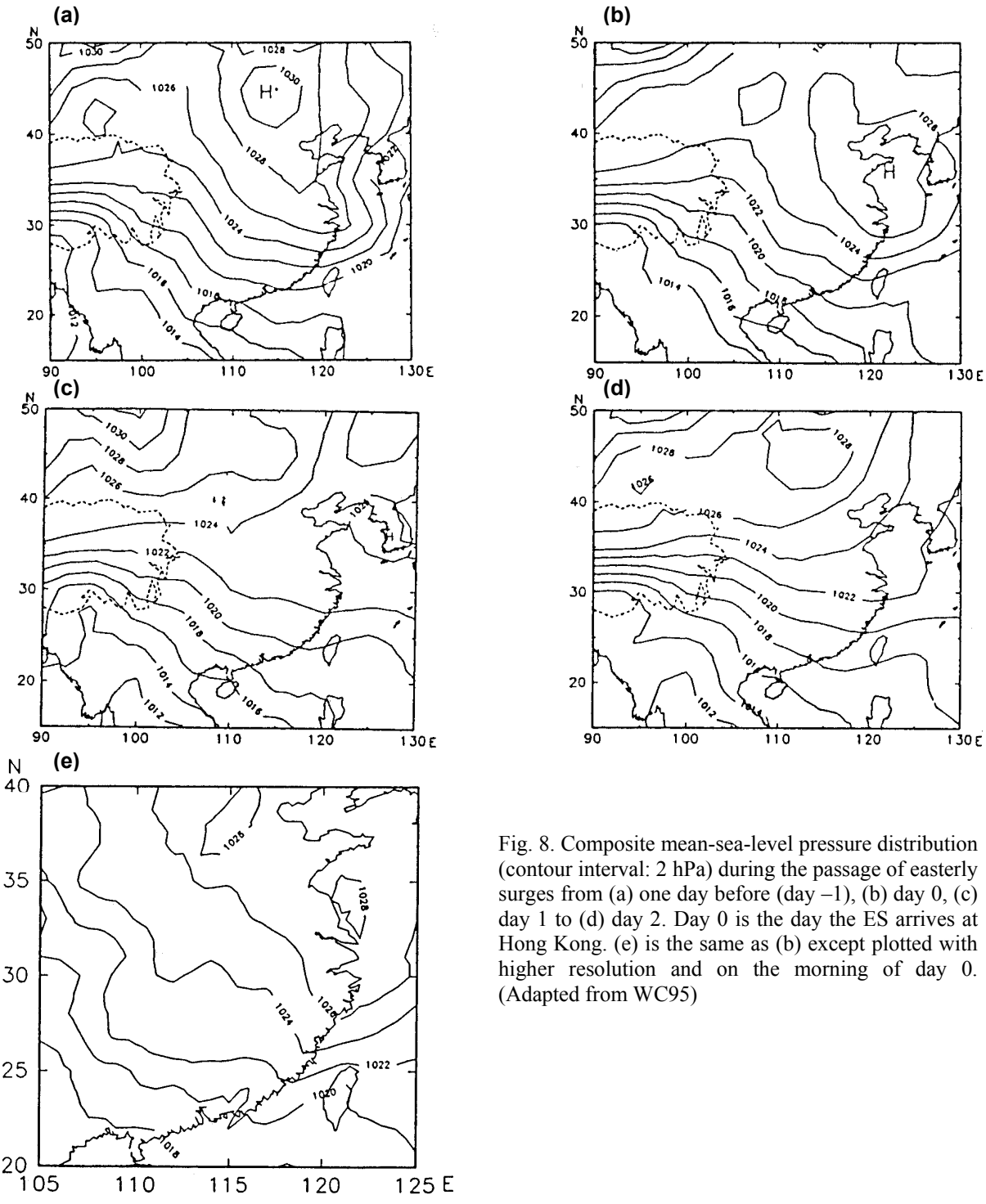

Fig. 8. Composite mean-sea-level pressure distribution (contour interval: 2 hPa) during the passage of easterly surges from (a) one day before (day –1), (b) day 0, (c) day 1 to (d) day 2. Day 0 is the day the ES arrives at Hong Kong. (e) is the same as (b) except plotted with higher resolution and on the morning of day 0. (Adapted from WC95)

Since the main trait of an ES is in the strengthening of the easterly winds (Morrice 1973), WC95 defined an ES as the strengthening of the easterly winds above a certain value. For the three-year data sample of WC95, the mean increase of the easterly component at Hong Kong from two days before (day –2) to the day of arrival day 0 of the ES is ~25 km h^{-1} with a standard deviation of ~ 5 km h^{-1}. On day 0, the mean wind is almost exactly easterly with an average magnitude of 43 km h^{-1}. Throughout the ES, the northerly component is < 10 km h^{-1}. Not much temperature drop can be identified in the case of ES, with the maximum decrease being less than 1°C at all locations along the coast (WC95).

The difference between an ES and an NS in the surface pressure distribution is in the location of the high-pressure cell center (cf. Figs. 2 and 8). In the case of ES, on day –1, the center is located near Dahingganling to the northwest of the Yellow Sea (Fig. 8a), with the mean central pressure of only around 1032 hPa. It then spreads southeastward (Fig. 8b) and reaches the Yellow Sea by day 0 (Fig. 8c). Notice that there appears to be a relative maximum in surface pressure along the east coast of China. Indeed, a careful examination of the pressure distribution on day 0 shows an obvious coastal ridging from Ningpo to Hong Kong (Fig. 8e). This appears to be similar to the ridging phenomenon found by Holland and Leslie (1986) along the Australian coast. By day 1, the horizontal pressure gradient has relaxed and the center of the high pressure moved to the Korean Peninsula (Fig. 8d), and the surge begins to subside.

The coastal ridging is apparently related to a coastal Kelvin-wave-type propagation along the east coast of China, as can be seen from the wind speed anomaly at various coastal stations (Fig. 9). The wind reaches a maximum about one and a half days before day 0. Moving along the coast southward, the maximum wind at Xiamen occurs about one day later. However, further southward propagation is not evident. Nevertheless, the winds over Hong Kong reach the maximum around day 0, by definition, although the easterlies apparently weaken rapidly so that at Yanjiang to the west of Hong Kong, not much increase in wind speed is observed.

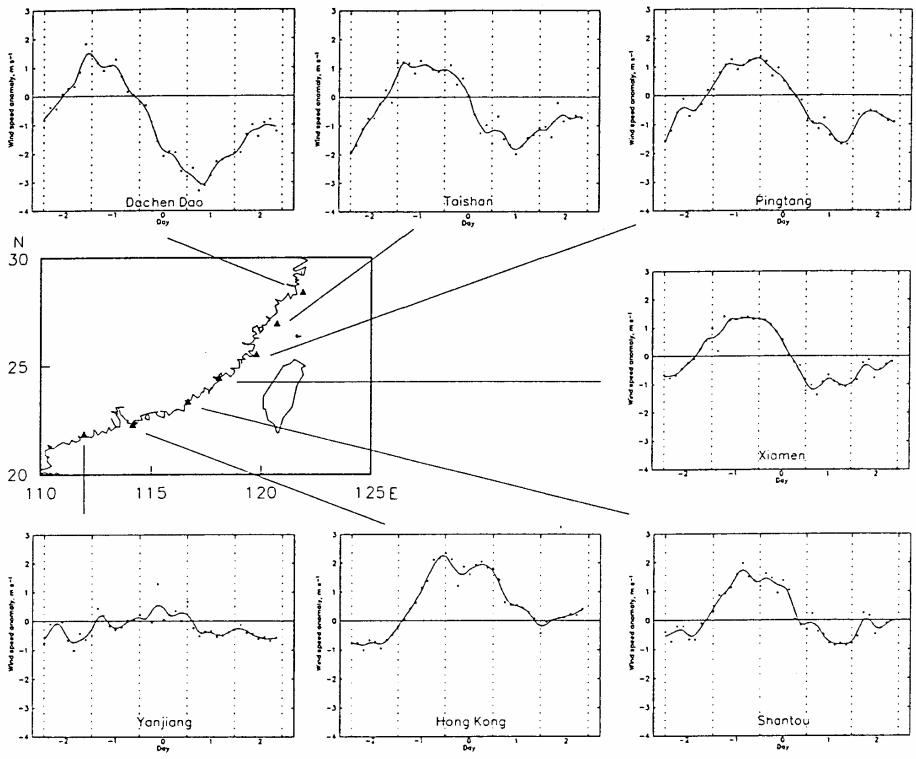

Fig. 9. Wind speed anomalies for seven selected coastal stations during an ES. The time interval is 3 h between the dots on each graph. (Adapted from WC95)

The origin of the surface high pressure is best identified from examining the 1000-hPa geopotential height distribution (Fig. 10). On day –3, the geopotential height of the SMH is ~ 290 gpm (Fig. 10a), which is slightly weaker than that for the NS. Then a clear split can be seen on day –2 (Fig. 10b), with the high over Dahingganling migrating southeastward (Fig. 10c), finally reaching the Shandong Peninsula by day 0 (Fig. 10d).

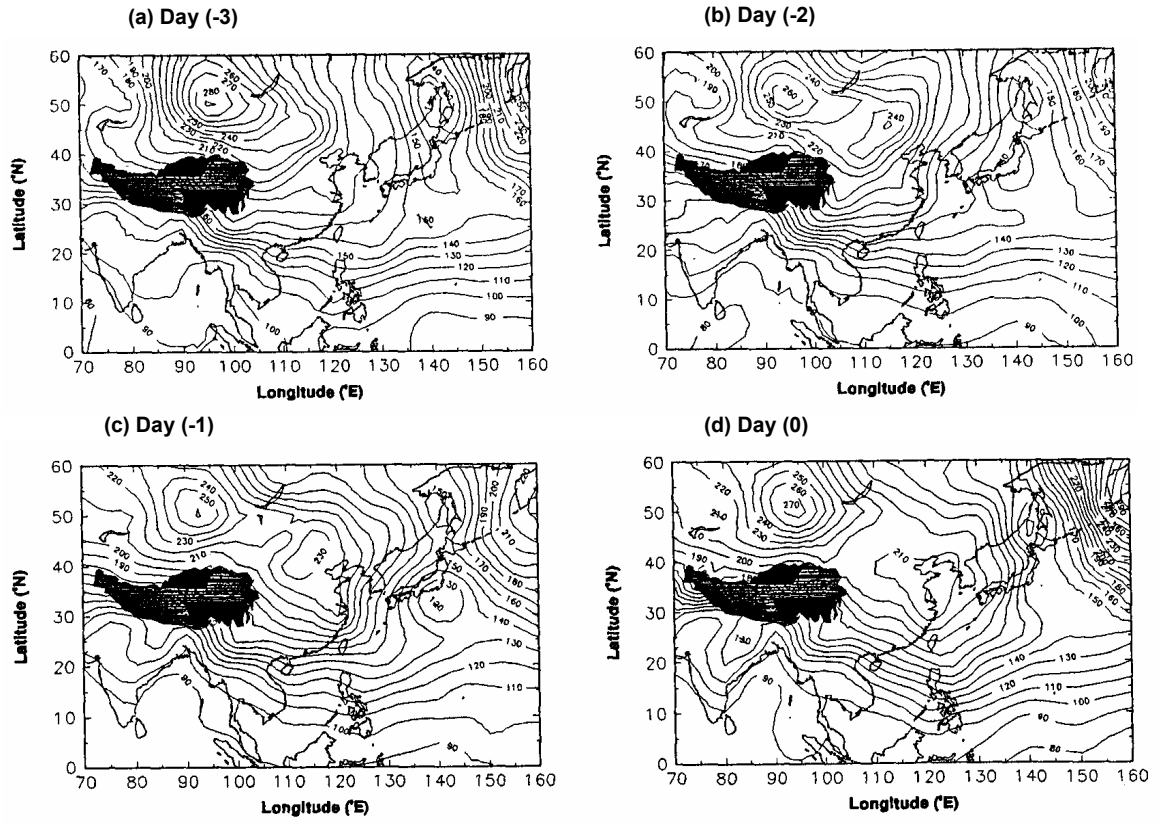

Fig. 10. Composite 1000-hPa geopotential heights (gpm) during an ES from day –3 to day 0. Contour interval: 10 gpm. Blackened area indicates the Tibetan Plateau with altitude greater than 3 km. (Adapted from WC97)

At 850 hPa, a broad anticyclone is seen over central China from day –2 (Fig. 11a). Notice that the center of this anticyclone is actually to the south of that at 1000 hPa, which indicates that the high is actually warm. Apparently, the subsidence warming associated with the Dahingganling high over-compensates the radiational cooling and cold advection. By day 0 (Fig. 11b), the 850-hPa flow is actually southerly over the mainland of China, which further causes warming in northern China (not shown – see WC97) and weakens the high. Note that the ridge axis at 850 hPa is almost oriented zonally along the south China coast on day 1 (Fig. 11c), which would bring in warm and moist air from the SCS. Indeed, an ES is generally associated with cloudy or even drizzly conditions over south China (Morrice 1973).

Up to now, the trigger of the split of the high from the SMH is still not clear. In addition, WC97 found that the jet stream is actually weakening in the case of ES and they suggested that perhaps barotropic instability might be responsible for the migration of the high due to a conversion of kinetic energy of the upper westerlies to that of the disturbance.

While the changes in the atmosphere associated with the ES do not appear as dramatic as those of the NS, it does present some interesting observations. An ES apparently results from the initially eastward and then southeastward migration of a cold pool that splits off from the quasi-stationary

SMH. Such a split appears to be related to the passage of a 500-hPa ridge over the SMH domain. As the low-level anticyclone moves to the east coast of China, it initiates a southward surge of cool air and strong winds along the coast, resembling a coastal Kelvin wave. By the time the wave reaches the south China coast, the winds strengthen to > 40 km h^{-1}. However, because the center of the anticyclone continues to move eastward, the winds cannot be maintained and therefore an ES is a short-lived surge. In addition, because of the shallow nature of the high, it weakens not only due to subsidence warming but also warm advection from the south.

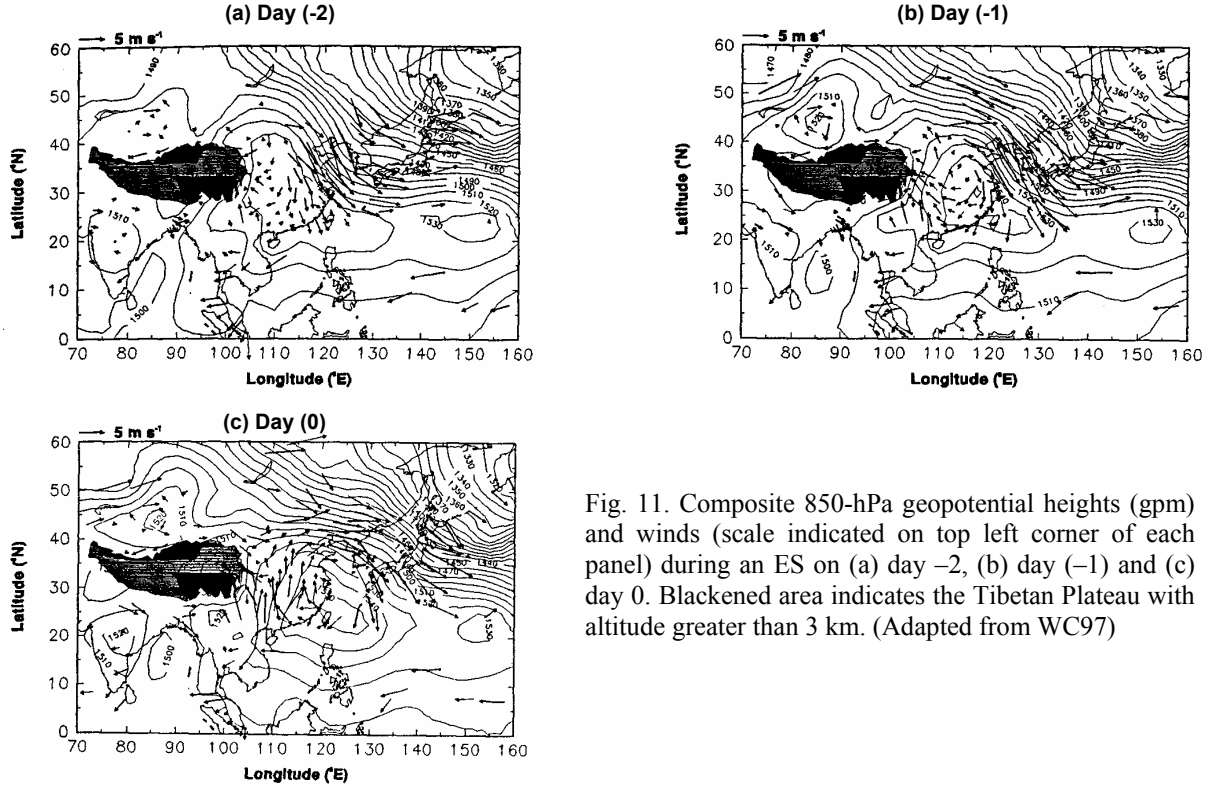

Fig. 11. Composite 850-hPa geopotential heights (gpm) and winds (scale indicated on top left corner of each panel) during an ES on (a) day –2, (b) day (–1) and (c) day 0. Blackened area indicates the Tibetan Plateau with altitude greater than 3 km. (Adapted from WC97)

2.3. Summary

The two types of surges presented in this section are obviously different, with the NS showing a much stronger synoptic signal and affecting a larger area. Nevertheless, the ES needs to be considered as well especially for the prediction of winds along the East China and South China coasts as well as the Taiwan Strait.

3. Explosive cyclogenesis off the East Asian continent

In addition to the monsoon surges described in the last section, an important feature of the winter monsoon is the often-explosive development of low-pressure systems off the East Asian coast associated with the eastward movement of the cold air off the continent. As the cold air encounters the relative warm ocean over the East China Sea, and the Kuroshio Current further east, a strong baroclinic zone is established. Rapid cyclogenesis often occurs. A similar situation occurs over the Atlantic as cold air moves off the North American continent and over the Gulf Stream (Sanders and Gyakum 1980).

Asai *et al.* (1988) showed three principal cyclone tracks in the East Asia region but only one group of cyclones along ~ 30°N is related to the EAWM. In most studies, a cyclone that deepens more than 24 hPa in 24 h is defined as an explosive cyclone, which follows the definition of Sanders and Gyakum (1980). Yi and Ding (1993) found that during the period 1973-88, about 20% of the EAWM-related cyclones went through the explosively deepening phase.

The latitudinal and longitudinal frequency distributions of explosive cyclones suggest a concentration near the latitude band of 30-35°N and the longitude band of 130-135°E (Fig. 12). This result suggests that while cyclones mostly develop off the East Asian coast (Hanson and Long 1985), they generally do not deepen explosively until they move near the Kuroshio Current south of Japan where the SST gradient is apparently the strongest. The distribution given in Fig. 12b for the area west of 130°E, which gives about 1 explosive cyclone per year, is consistent with that of Dong and Li (1989) based on the data from 1966-85. Note, however, the average number of explosive cyclones is around 10 per year. If the origin of the cyclones is not considered, the number of explosive events over the entire western North Pacific reaches about 20 per year (Ouyang *et al.* 1990), which implies that half of the explosive cyclones are associated with the EAWM.

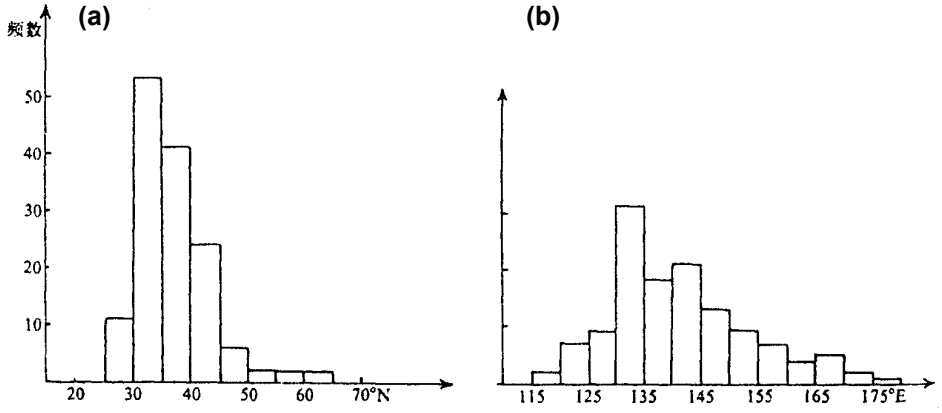

Fig. 12. (a) latitudinal (averaged between 115–180°E), and (b) longitudinal (averaged between 20–70°N) distributions of the number of explosive cyclones originating from China at the initial time of their explosive deepening phase during the period 1973–1988. (from Yi and Ding 1992)

While it might be expected the explosive events occur mostly in winter, the monthly distribution of the absolute maximum actually occurs in March (not shown). The total frequencies of occurrence for the winter (December to February) and spring (March to May) months are about equal. The distributions of the total number of cyclones around similar regions found by Hanson and Long (1985) and Asai *et al.* (1988) also give a maximum frequency in March and April (not shown).

Yi and Ding (1993) also classified the intensity of explosive cyclones based on the scale proposed by Sanders (1986). They found that west of 130°E, strong cyclones (> 1.8 Bergeron1) occur only about once every 5 years, but the frequency of occurrence between 130 and 180°E is close to 1.5 per year.

Most of the observational or numerical investigations of the physical processes associated with the genesis and development of explosive cyclones are based on case studies. Even when many cases were included (e.g. Li and Ding 1989; Sun and Gao 1993), the diagnoses were performed on one or two specific cyclones. In all the studies, latent heat release is identified as the crucial factor in

[1] 1 Bergeron = 24 hPa/24 h x (sin ϕ/sin 60°), where ϕ is the latitude of the center of the cyclone (Sanders 1986).

determining whether a cyclone can deepen explosively. In a numerical study of the explosive development of a cyclone over the Kuroshio Current, Xu and Zhou (1999) found that by turning off latent heating, the deepening of the simulated cyclone was much less. Chen and Dell'Osso (1987) obtained similar results in a case study of a cyclone that deepened ~ 20 hPa in 24 h. Without latent heating, the modeled cyclone remained a shallow feature. The diagnostic analyses of Li and Ding (1989) and Yi and Ding (1992) also found the magnitude of latent heating to be the maximum during the explosive developing phase of these cyclones.

The latent heat release necessary for the development of these cyclones is generally attributed to the presence of strong rising motion. Mechanisms that are apparently responsible for causing the ascent include low-level convergence due to sensible heating of the boundary layer, upper-level divergence and positive vorticity advection due to the passing of a shortwave trough, vertical differential temperature advection, and secondary circulation at the exit region of a passing subtropical jet streak (e.g. Li and Ding 1989; Yi and Ding 1992; Sun and Gao 1993). Horizontal advection of heat and moisture into the low-pressure system by an ageostrophic low-level jet has also been identified as a mechanism that increases the instability of the atmosphere to allow the conversion of available potential energy to eddy kinetic energy of the cyclone. The latent heating not only provides the energy necessary for the development of the system, but can also feed back to amplify either the shortwave trough (Xu and Zhou 1999) or the jet streak circulation (Chen and Dell'Osso 1987). It also enhances the rising motion and thus creates a positive feedback process, and hence an explosive development.

4. Temporal variations of the EAWM

4.1. Synoptic to interdecadal variations of the winter monsoon

While the winter monsoon is always a dominant climate system in the East Asia/western North Pacific region every year, its activity in terms of frequency of occurrence and intensity varies during different months of the winter season. Previous studies have identified a 6-8-day period associated with the cold-air outbreaks (Tao 1959; Murakami 1979). A spectral analysis of the 1000-hPa meridional winds over the East Asia/western North Pacific region (20-30^{o}N, 120-150^{o}E) indeed shows a peak of 5-8 days (Fig. 13). A similar analysis of the intensity of winter monsoon also shows a similar period.

Another peak with a 10-20 day period is also evident from Fig. 13. This quasi-biweekly oscillation has also been found in some previous studies (Pan and Zhou 1985; Chen and Xie, 1988). Variations of the EAWM on this time scale are mainly associated with the evolution of the blocking pattern of atmospheric circulation in the midlatitudes especially in the Ural mountain region, where the NS originates (see section 2.1).

On a slightly longer time scale, intraseasonal variations of the EAWM have also been identified (Li 1989a; Zhu *et al.* 1990). As an example, the temporal variation of surface temperature anomalies at Guangzhou in southern China shows a clear intraseasonal (30-60 day) oscillation (Fig. 14). Such oscillations are also apparent at the mid troposphere. In stronger EAWM years (e.g. 1971-72), the negative height anomalies can propagate very close to the equator (Li 1989a) than those in weaker EAWM years (e.g. 1966-67). It also means that the intraseasonal (30-60 day) variation is an important feature of the EAWM activity.

As discussed in section 3, the meridional wind in the lower troposphere in the East Asia/western North Pacific region is a good indicator to represent the activity of the EAWM. By examining the temporal variation and power spectrum of the surface meridional wind anomalies averaged within the region (20-30^{o}N, 120-150^{o}E), Mu and Li (1999) found strong interannual variations with two major

cycles: 2-year and 4-7-year (Fig. 15). The two-year cycle might suggest some type of biennial oscillation and the 4-7-year cycle is likely to be related to ENSO. They also found suggestions of 7-10 and 20-30-year periods.

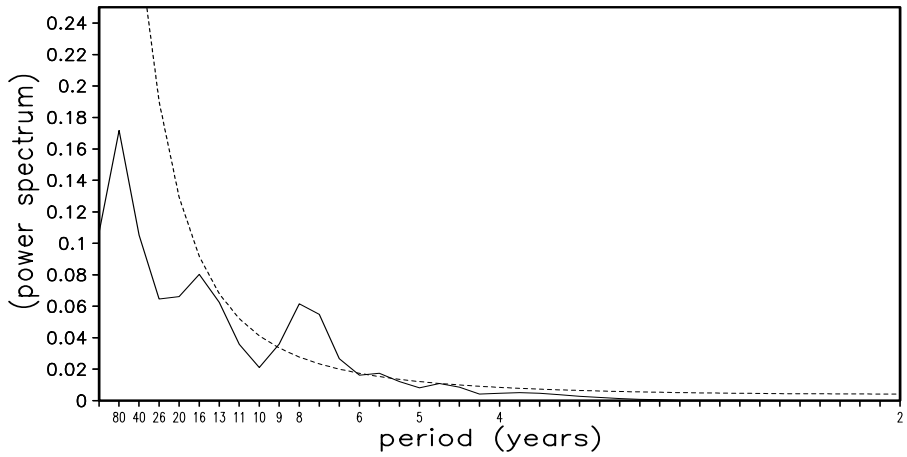

Fig. 13. Power spectrum of 1000-hPa meridional winds averaged in the East Asia region (20°–30°N, 120°–150°E). The dashed curve shows the 95% confidence level (Chan and Li 2004).

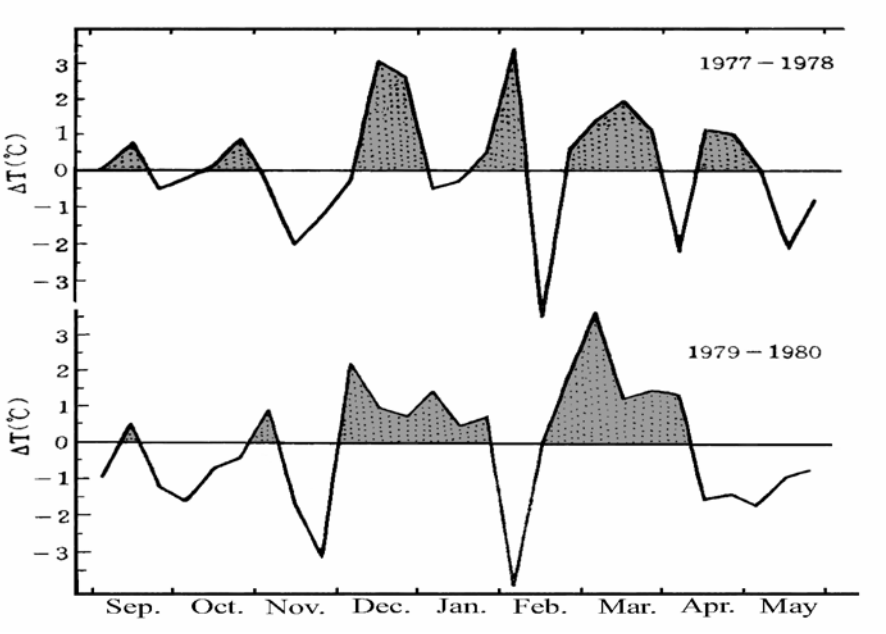

Fig. 14. Temporal variation of the 10-day averaged surface temperature anomalies at Guangzhou station (from Li 1989a).

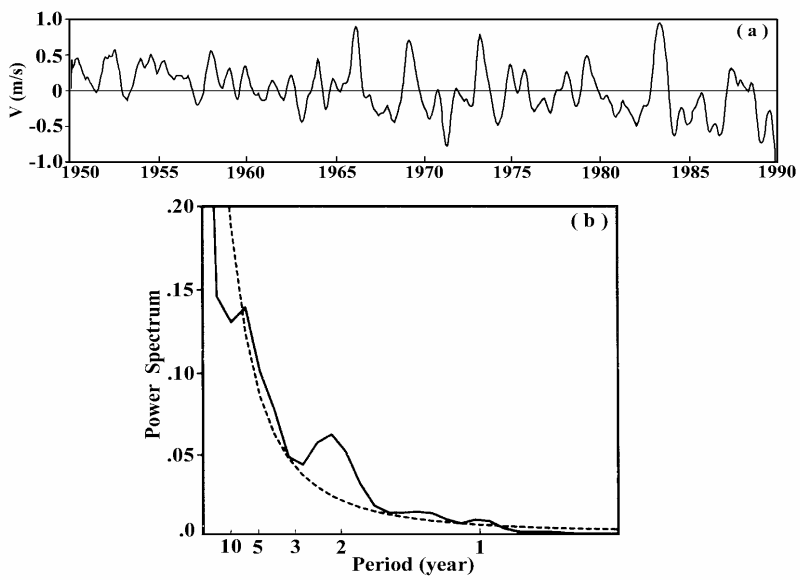

Fig. 15. (a) Temporal variation and (b) power spectrum of the surface meridional wind anomalies in the (20–30°N, 120–150°E) region. The dashed curve in (b) shows the 95% confidence level (from Mu and Li 1999).

4.2. Relationship between EAWM and ENSO

The interaction between the EAWM and ENSO has been studied extensively. On the one hand, an anomalous East-Asian winter monsoon is a necessary (though not sufficient) condition for the occurrence of a warm ENSO event (Li *et al.* 1989; Li and Mu 1998; Xu and Chan 2001). On the other hand, a warm (cold) ENSO event can weaken (enhance) the EAWM through remote response and teleconnection. In this sub-section, only the latter is discussed.

Li (1989b, 1995) showed that a warm winter (weak EAWM) usually occurs in East Asia during the developing to mature phase of an El Niño year but the reverse occurs during a La Niña year. Two processes may be responsible for the influence of ENSO on the EAWM. Firstly, the Hadley and Ferrel cells are both enhanced (reduced) during an El Niño (a La Niña) event (Wu and Cubasch 1987; Li 1990b). As a result, the westerlies in the mid latitudes are strengthened (weakened), which then limits (enhances) the development of the 500-hPa trough over East Asia. Secondly, an anomalous anticyclonic (cyclonic) circulation usually exists over the western Pacific to the east of the Philippines during the El Niño (La Niña) winter (Wang *et al.* 2000). The anomalous southerlies (northerlies) will therefore weaken (enhance) the cold outbursts towards the south in East Asia and the western North Pacific region.

Wu and Chan (2000) compared the intensity of the winter monsoon over South China in ENSO and non-ENSO years, and found the results to be largely consistent with those for the whole of China. That is, in the winter during the mature phase of a warm (cold) event, the EAWM tends to be weak (strong) while no coherent signal can be detected in non-ENSO years, which suggests that factors other than ENSO also control the interannual variability of the EAWM.

4.3. Other factors to affect variations of the EAWM

In addition to ENSO, some other atmospheric phenomena or oscillations have been found to be

related to the intensity of the EAWM. These include the polar vortex (Chan and Li 2004), SSTA in the North Pacific (Li and Xian 2002), the North Atlantic Oscillation (Wu and Huang 1999) and the East Asia summer monsoon (Wu and Chan 1997; Wu 2002). Causality in most of these relationships has, however, not been fully identified. Therefore, they will not be discussed in detail in this review. Interested readers can refer to the original papers.

5. Discussion and unresolved issues

Compared with its counterpart – the summer monsoon, the EAWM has not received as much attention because its impact on society is perceived to be not as large. Therefore, the amount of research in the study of the EAWM is much less. However, as evidenced by the discussion here, the effects of the EAWM could just be as hazardous. Thus, more research efforts should be devoted to the study of the EAWM, in particular, the identification of the physical mechanisms that link the EAWM and other atmospheric and oceanographic phenomena. In addition, while the two types of surges have been documented, the results have been based on a relatively small dataset. With the recent availability of different reanalyses datasets, it should be possible to re-evaluate the physical hypotheses put forward to describe the physical mechanisms of the surges, especially for the easterly surges. Further studies of the explosive cyclogenesis should also be performed given the amount of satellite data currently available.

Acknowledgments

Much of the material presented here is excerpted from a chapter written by the author and Prof. Chongyin Li in the forthcoming book *East Asia Monsoon* edited by Prof. C. P. Chang to be published by World Scientific.

References

Asai, T., Y. Kodama and J.-C. Zhu, 1988: Long-term variations of cyclone activities in East Asia. *Adv. Atmos. Sci.*, **5,** 149-158.

Boyle, J. S. and T. J. Chen, 1987: Synoptic aspects of the wintertime East Asian monsoon. *Monsoon Meteorology*, C. P. Chang and T. N. Krishnamurti (Eds.), Oxford Univ. Press, 125-160.

Chan, J. C. L. and C. Li, 2004: The East Asia winter monsoon. *East Asia Monsoon*, C. P. Chang (Ed.), World Scientific (forthcoming).

Chang, C. P. and K. M. Lau, 1980: Northeasterly cold surges and near-equatorial disturbances over the winter MONEX area during December 1974. Part II: Planetary-scale aspects. *Mon. Wea. Rev.*, **108,** 298-312.

Chang, C. P., J. E. Millard and G. T. J. Chen, 1983: Gravitational character of cold surges during winter MONEX. *Mon. Wea. Rev.*, **111,** 293-307.

Chen, L. and A. Xie, 1988: Westward propagating low-frequency oscillation and its teleconnection in the Eastern Hemisphere. *Acta Meteor. Sinica*, **2,** 300-312.

Chen, Q. and A. Huang, 1989: Some features of the South China Sea cold surge during winter season. *Meteor. Monthly*, **15,** 49-53. (in Chinese with English abstract)

Chen, S.-J. and L. Dell'Osso, 1987: A numerical case study of East Asian coastal cyclogenesis. *Mon. Wea. Rev.*, **115,** 477-487.

Compo, G. P., G. N. Kiladis and P. J. Webster, 1999: The horizontal and vertical structure of east Asian winter monsoon pressure surges. *Quart. J. Roy. Meteor. Soc.*, **125,** 29-54.

Davidson, N. E., J. L. McBride and B. J. McAvaney, 1983: The onset of the Australian monsoon during winter MONEX: Synoptic aspects. *Mon. Wea. Rev.*, **111,** 495-516.

Ding, Y., 1990a: Build-up, air mass transformation and propagation of Siberian high and its relation to cold surge in East Asia. *Meteor. Atmos. Phys.*, **44,** 281-292.

Ding, Y., 1990b: A statistical study of winter monsoons in East Asia. *J. Tropical Meteor.*, **6,** 119-128. (in Chinese with English abstract)

Ding, Y., 1994: *Monsoons over China.* Kluwer Academic Publishers, 419pp.

Ding, Y. and T. N. Krishnamurti, 1987: Heat budget of the Siberian high and the winter monsoon. *Mon. Wea. Rev.*, **115,** 2428-2449.

Ding, Y. and M. Xiao, 1992: A case study of development and structure of a cold surge in East Asia. *Proc., 2nd Int'l Conf. East Asia and Western Pac. Meteor. and Climate*, W. J. Kyle and C. P. Chang (Eds.), World Scientific, 311-328.

Dong, L. and D. Li, 1989: Coastal and oceanic explosive cyclones to the east of China. *Acta Meteor. Sinica*, **47,** 371-375. (in Chinese with English abstract)

Hanson, H. P. and B. Long, 1985: Climatology of cyclogenesis over the East China Sea. *Mon. Wea. Rev.*, **113,** 697-707.

Holland, G. J. and L. M. Leslie, 1986: Ducted coastal ridging over S. E. Australia. *Quart. J. Roy. Meteor. Soc.*, **49,** 428-438.

Holton, J. R., 1992: *An Introduction to Dynamic Meteorology.* 3rd ed., Academic Press, 507pp.

Li, C., 1989a: Frequent activities of stronger upper-level troughs in East Asia in wintertime and the occurrence of the El Nino event. *Science in China (B)*, **32,** 976- 985.

Li, C., 1989b: Warmer winter in Eastern China and El Nino. *Chinese Science Bulletin*, **34**, 1801-1805.

Li, C., 1990a: Interaction between anomalous winter monsoon in East Asia and El Niño events. *Advances in Atmos. Sci.*, **7,** 36-46.

Li, C., 1990b: On interaction between anomalous circulation/climate in East Asia and El Niño event. *Climate Change Dynamics and Modeling,* China Meteorological Press, Beijing. 101-126.

Li C., 1995: *Introduction to Climate Dynamics*. China Meteorological Press, Beijing, 461 pp. (in Chinese)

Li, C. and Y. Ding, 1989: A diagnostic study of an explosively deepening oceanic cyclone over the northwest Pacific Ocean. *Acta Meteor. Sinica*, **47,** 180-190. (in Chinese with English abstract)

Li C., Y. Chen and Z. Yuan, 1989: Important cause of El Nino events – Frequent activities of stronger cold waves in East Asia. *Frontiers in Atmospheric Sciences*, New York: Allenton Press, 156-165

Li C. and M. Mu, 1998: Numerical simulations of anomalous winter monsoon in East Asia exciting ENSO. *Chinese J. Atmos. Sci.*, **22**, 393-403.

Li, C., and P. Xian, 2002: The influence of interdecadal mode of North Pacific SST on climate anomalies. *Adv. Atmos. Sci.*, (to be published).

Lim, H. and C. P. Chang, 1981: A theory for midlatitude forcing of tropical motions during winter monsoons. *J. Atmos. Sci.*, **38,** 2377-2392.

Love, G., 1985: Cross-equatorial influence of winter hemisphere subtropical cold surges. *Mon. Wea. Rev.*, **113,** 1487-1498.

Morrice, A. M., 1973: Quantitative forecasting of the winter monsoon in Hong Kong. *Tech. Note No. 35*, Royal Observatory Hong Kong, 41 pp.

Mu, M. and C. Li, 1999: ENSO signals in interannual variability of East Asian winter monsoon, Part I: Observed data analyses. *Chinese J. Atmos. Sci.,* **23,** 134-143.

Murakami, T., 1979: Winter monsoonal surge over East and Southeast Asia, *J. Meteor. Soc. Japan*, **57**, 133-158.

Ouyang, Z., M. Lu and Z. Hu, 1990: Some statistical characteristics of explosive cyclones in Asian and northwest Pacific. *J. Air Force Meteor.*, **11,** 23-30. (in Chinese)

Palmén, E. and C. W. Newton, 1969: *Atmospheric Circulation Systems – Their Structure and Physical Interpretation.* Int'l Geophys. Series No. 13, Academic Press, 603 pp.

Pan, H. L., and F. X. Zhou, 1985: The 10-20 day tropical-midlatitude interaction during winter monsoon season. *J. Meteor. Soc. Japan,* **63**, 829-843.

Qiu, Y., X. Li and Y. Qiu, 1992: Statistical features of the cold waves invaded China and their relation to the snow cover area over the Eurasian continent. *Quart. J. Appl. Meteor.*, **3,** 235-241. (in Chinese with English abstract)

Sanders, F., 1986: Explosive cyclogenesis in the west central North Atlantic Ocean, 1981-1984. *Mon. Wea. Rev.*, **114,** 1781-1794.

Sanders, F., and J. R. Gyakum, 1980: Synoptic dynamic climatology of the "bomb". *Mon. Wea. Rev.*, **108,** 1589-1606.

Sun, S. and S. Gao, 1993: The effect of East Asia cold surge activity on the downstream genesis of explosive cyclones. *Acta Meteor. Sinica*, **51,** 304-313. (in Chinese with English abstract)

Tao, S., 1959: East-Asian Cold Wave Research in China during Recent 10 Years. *Acta Meteorologica Sinica*, **30**, 226-230. (in Chinese).

Wang, B., R. Wu, and X. Fu, 2000: Pacific–East Asian teleconnection: How does ENSO affect East Asian climate? *J. Climate,* **13**, 1517-1536.

Wu, B. and R. Huang, 1999: Effects of the Extremes in the North Atlantic oscillation on East Asia winter monsoon. *Chinese J. Atmos. Sci.*, **23,** 641-651.

Wu, G., and U. Cubasch, 1987: The impact of the El Niño anomaly on the mean meridional circulation and atmospheric transformations. *Scientia Sinica,* Series B, **30,** 533-545.

Wu, M. C., 2002: Relationship between winter and summer and monsoons over East Asia. *Ph.D. Thesis*, City University of Hong Kong, 228pp.

Wu, M. C. and J. C. L. Chan, 1995: Surface features of winter monsoon surges over South China. *Mon. Wea. Rev.*, **123,** 662-680.

Wu, M. C. and J. C. L. Chan, 1997: Upper-level features associated with winter monsoon surges over South China. *Mon. Wea. Rev.*, **125,** 317-340.

Wu, M. C. and J. C. L. Chan, 2000: Winter monsoon over South China in ENSO and non-ENSO years. *Preprints, 24th Conf. Hurr. Trop. Meteor.*, Amer. Meteor. Soc., 29 May – 2 June, Ft. Lauderdale, Florida, USA, 110-111.

Xu, J. and J. C. L. Chan, 2001: The role of the Asian/Australian monsoon system in the onset time of El Niño events. *J. Climate*, **14,** 418-433.

Xu, Y. and M. Zhou, 1999: Numerical simulations on the explosive cyclogenesis over the Kuroshio Current. *Adv. Atmos. Sci.*, **16,** 64-76.

Yi, Q. and Y. Ding, 1992: A dynamic study of two explosively deepening cyclones over the East China Sea. *Acta Meteor. Sinica*, **50,** 152-166. (in Chinese with English abstract)

Yi, Q. and Y. Ding, 1993: Climatology of the explosive cyclogenesis over East Asia and the west Pacific. *Sci. Atmos. Sinica*, **17,** 302-309. (in Chinese with English abstract)

Zhang, P. and G. Chen, 1999: A statistical analysis of the cold wave high which influences China. *Acta Meteor. Sinica*, **57,** 493-501. (in Chinese with English abstract)

Zhang, Y., K. R. Sperber and J. S. Boyle, 1997: Climatology and interannual variation of the East Asian winter monsoon: Results from the 1979-95 NCEP/NCAR Reanalysis. *Mon. Wea. Rev.*, **125,** 2605-2619.

Zhao, Q. and Y. Ding, 1991: A study of physical processes affecting the transformation of cold air over land after outbreak of cold waves in East Asia. *Acta Meteor. Sinica*, **49,** 170-180. (in Chinese with English abstract)

Zhou, X., 1989: An analysis of two cold surges. *J. Trop. Meteor.*, **5,** 57-63. (in Chinese with English abstract)

Zhu, Q., X. Zhi and Z. Lei, 1990: Low frequency summer monsoon in Indonesia-Northern Australia and its relation to circulation in both Hemispheres. *Acta Meteor. Sinica,* **4,** 543-553.

MARITIME CONTINENT MONSOON

C.-P. CHANG

Department of Meteorology
Graduate School of Engineering and Applied Sciences
Naval Postgraduate School, Monterey, CA93943, USA
E-mail: cpchang@nps.edu

(The review here is based on the abstract and figures of "Chapter 3: Maritime Continent Monsoon," by C.-P. Chang, P. A. Harr and J. M. McBride, in the book "East Asian Monsoon", World Scientific Series on Meteorology of East Asia, Volume 2, World Scientific, 2004.)

Abstract

The Maritime Continent and northern Australia is a region of strong seasonal variation in wind and rainfall regimes, which consist of a prevailing easterly wind and dry conditions during the boreal summer and prevailing westerly winds and wet conditions during the boreal winter. During the boreal winter, latent heat release associated with the wet season over the Maritime Continent and northern Australia contributes to a major component of the global circulation, which has been linked to significant tropical-extratropical interactions. Although substantial research has been conducted with respect to the northern Australia component of the boreal winter monsoon, the variations associated with the Maritime Continent component of the large-scale monsoon system have received less attention. In this Chapter, the annual cycle of rainfall and the interannual, sub-seasonal, and synoptic variabilities associated with the boreal winter monsoon over the Maritime Continent are described.

The equator serves as a general demarcation between the boreal summer (to its north) and boreal winter (to its south) monsoon rainfall regimes. However, locally the annual cycle is dominated by interactions between the complex terrain and an annual reversal of the surface winds. These interactions cause the summer and winter monsoon regimes to intertwine across the equator. In particular, the boreal winter regime extends far northward along the eastern flanks of the major island groups and landmasses. There is no complementary extension of the boreal summer regime into southern latitudes. The seasonal march is asymmetric during the transitional seasons, with the maximum convection following a gradual southeastward progression from the Asian summer monsoon to the Asian winter monsoon but a sudden transition in the reverse. This asymmetric march is explained by a hypothesis based on the redistribution of mass between land and ocean areas during spring and fall that results from different land-ocean thermal memories. This mass redistribution produces sea-level pressure patterns that lead to asymmetric wind-terrain interactions throughout the region, and a low-level divergence asymmetry in the region that promotes the southward march during boreal fall but opposes the northward march during boreal spring.

Interannual variability in boreal winter Maritime Continent monsoon rainfall is examined with respect to the El Nino-Southern Oscillation (ENSO). Significant variability in the ENSO-monsoon relationship exists across the Maritime Continent and its vicinity, particularly between the Sumatra-Malay Peninsula-western Borneo region and regions to its east and west. A significant part of this variability is linked to the influence of the Walker Circulation and its variations between warm and cold ENSO events. There is also evidence of interdecadal changes in the ENSO-monsoon relationship and its variability.

Both boreal summer and boreal winter rainfall in the Maritime Continent rainfall exhibit signals of the Tropical Biennial Oscillation. Atmosphere-ocean interaction processes appear to play an important role in the production of these signals.

Sub-seasonal and synoptic variability in boreal winter Maritime Continent rainfall is examined with respect to the Madden-Julian Oscillation (MJO), northeasterly cold surges, and the Borneo Vortex. Relationships among all three circulation systems are found to have significant impacts on large-scale atmospheric conditions that impact the spatial distribution of rainfall throughout the region. Convection over the southern South China Sea is strongest during the combination of a northeasterly surge and Borneo vortex. However, the frequency of surges is reduced when the MJO is present.

1. Introduction

2. Annual Cycle and Seasonal March of Rainfall

2.1 Annual Variation of Rainfall, Monsoon Onset and Withdrawal

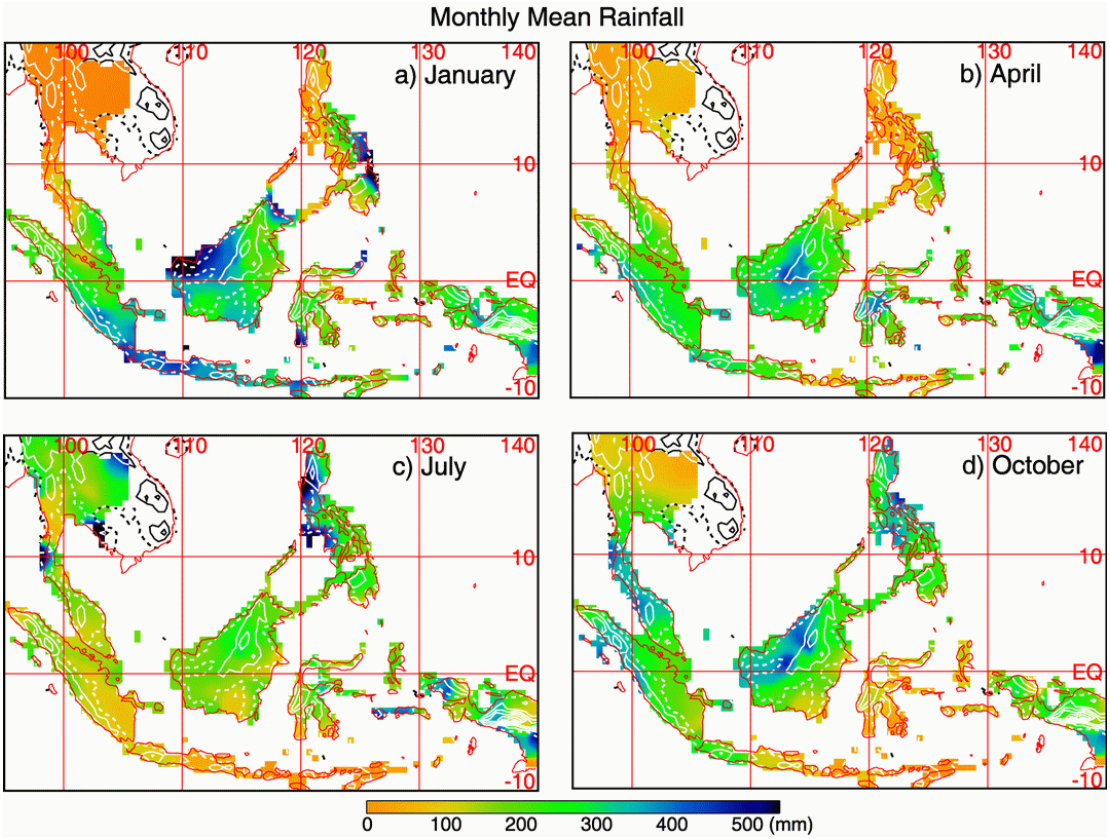

Figure 1. Monthly mean rainfall and topography for (a) January, (b) April, (c) July, and (d) October. Data are analyzed from long-term station rainfall reports of various periods with minimum length of 48 years.

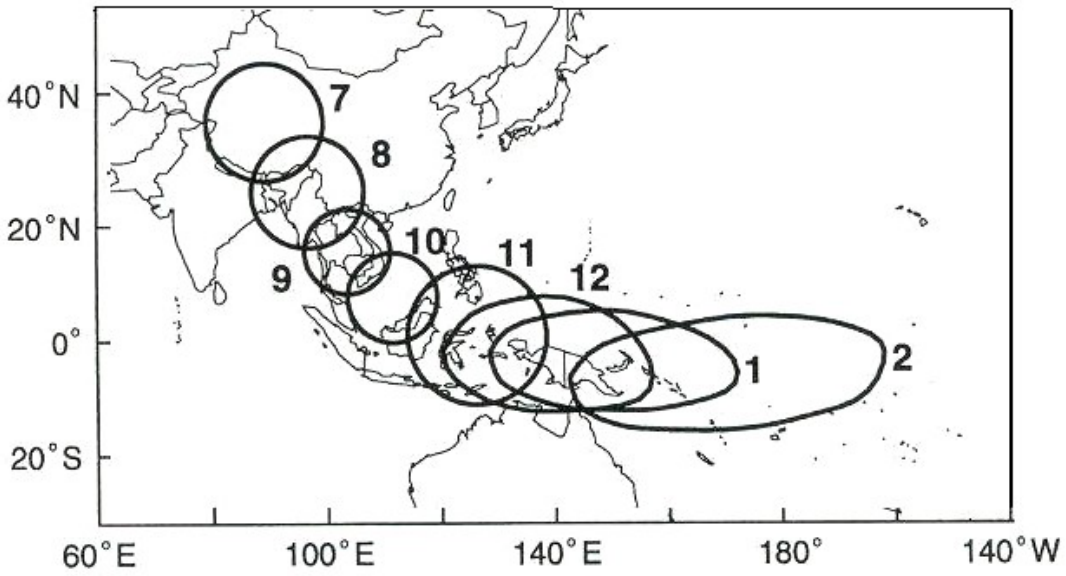

Figure 2. Seasonal migration of the monsoon diabatic heat sources during July-February (denoted by marching numerals). The extent of the diabatic heat sources is determined from the area with OLR < 225 W m^{-2} from monthly OLR climatology and is approximately proportional to the size and orientation of the schematic drawings. (Adapted from Lau and Chan 1983).

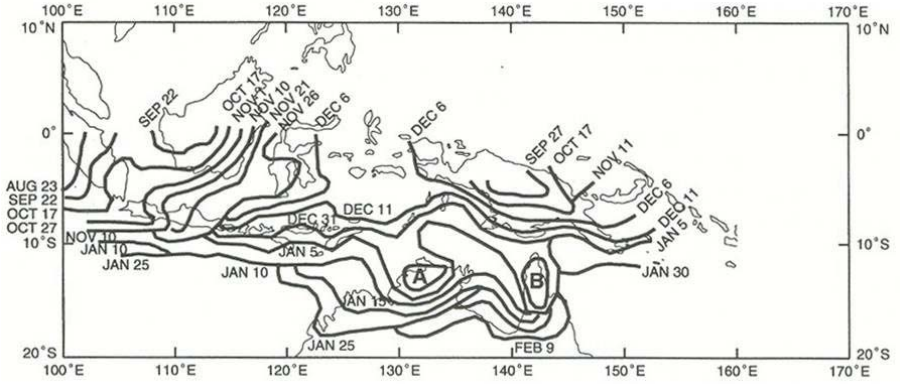

Figure 3. Monsoon onset dates defined by the threshold value of more than 30% of the mean high cloud amount for the monsoon season. Regions A and B had onset prior to 15 December and 26 December, respectively. (Adapted from Tanaka 1994).

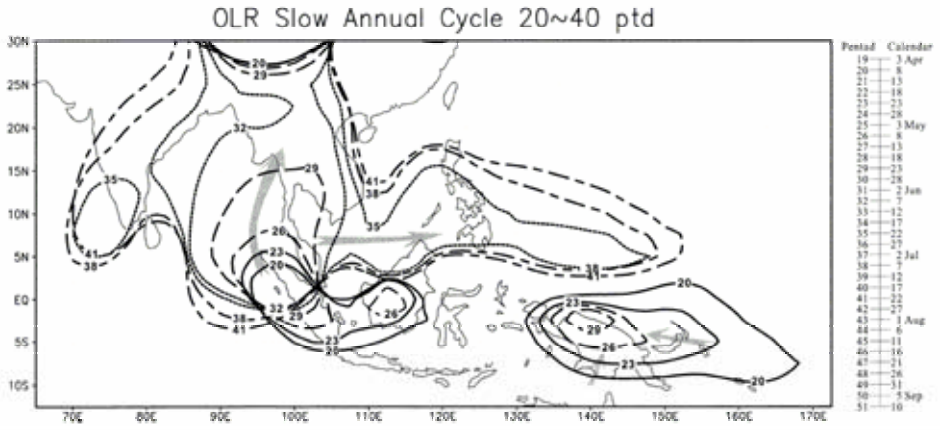

Figure 4. The slow annual cycle of areas enclosed by OLR ≤ 220 W m^{-2}, labeled by pentad. (From LinHo and Wang 2002).

2.2 Annual Cycle and Semiannual Cycle Modes for Rainfall

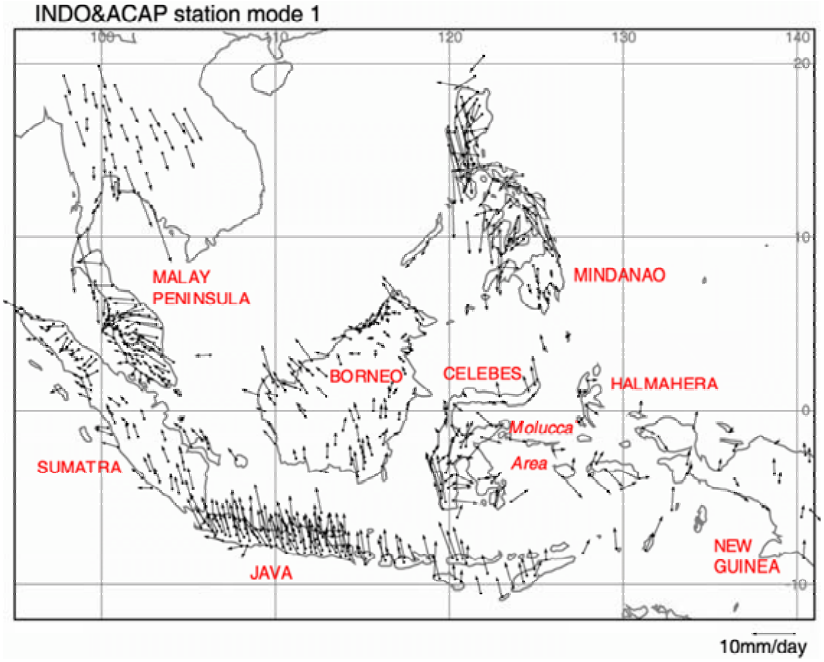

Figure 5. The annual cycle mode at rainfall stations. The phase of the cycle is shown as a 12-month clock with a northward arrow indicating maximum rainfall in January. The arrows rotate clockwise with eastward, southward and westward arrows indicating April, July and October, respectively. The length of the arrow defines the amplitude of the cycle. (From Chang *et al.* 2004c).

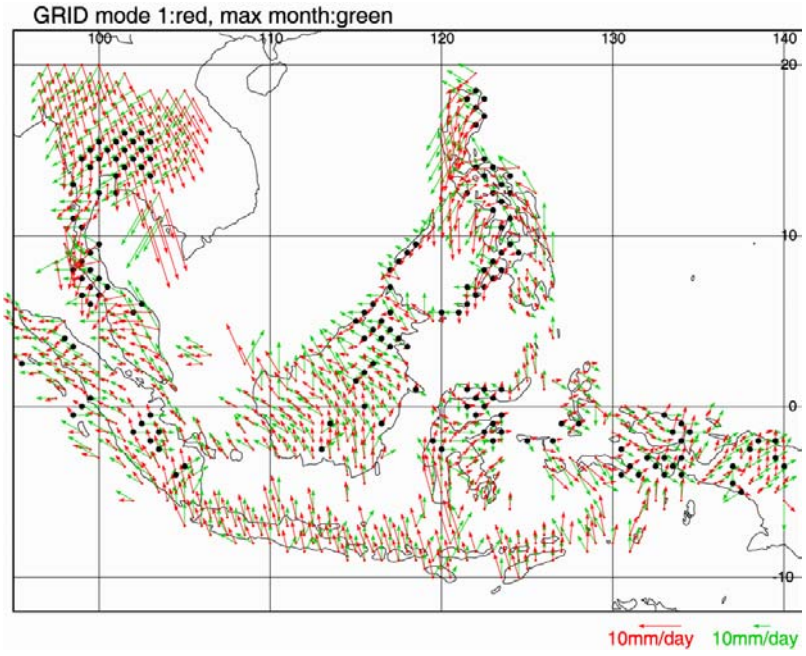

Figure 6. The annual cycle mode (red) and the month and amount of the maximum monthly rainfall (green) for the objectively-analyzed gridded rainfall. The maximum monthly rainfall arrows are scaled to 1:4 of the annual cycle arrows. Black dots indicate grid points where the amplitude of the annual cycle mode is no more than 40% of the maximum rainfall and the phase difference is at least two months. (From Chang *et al.* 2004c).

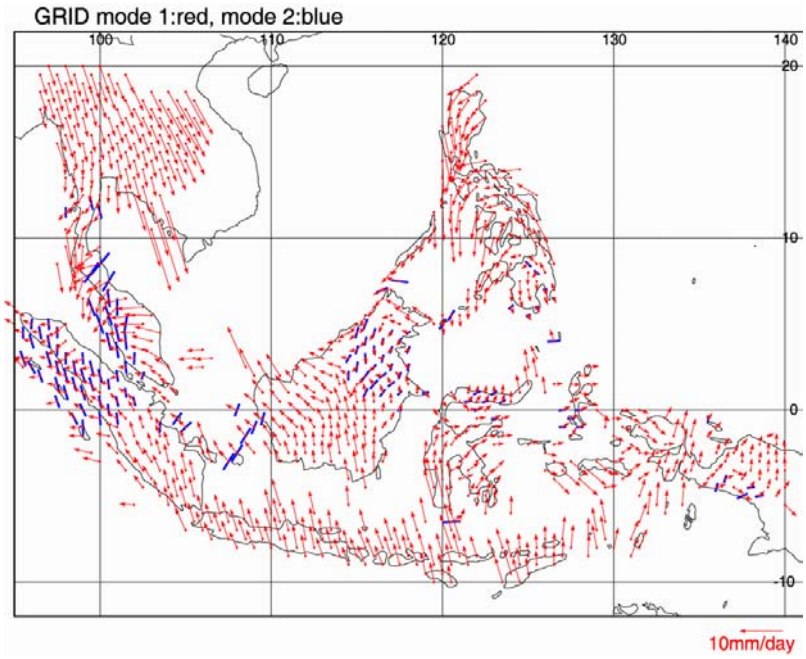

Figure 7. The semiannual cycle mode (blue bar), overlapped with the annual cycle mode (red), for the objectively-analyzed gridded rainfall. Data are plotted if the amplitude of the semiannual cycle is at least 80% of that of the annual cycle. Each bar is centered at the grid point and pointing in the two (opposite) directions of the semiannual cycle peaks. A vertical (north-south) bar indicates rainfall maximum in winter and summer and a horizontal (east-west) bar indicates rainfall maximum in spring and fall. The entire length of the bar is twice the length of an annual cycle vector with the same amplitude. Example of rainfall time series (mm day^{-1}) at grid points where the semiannual cycle is important (5°N, 100°E), the annual cycle is important (8°S, 110°E), and neither is important (3°S, 133.5°E) are shown in the upper-right insert. (From Chang *et al.* 2004c).

2.3 Boreal Summer and Winter Monsoon Regimes

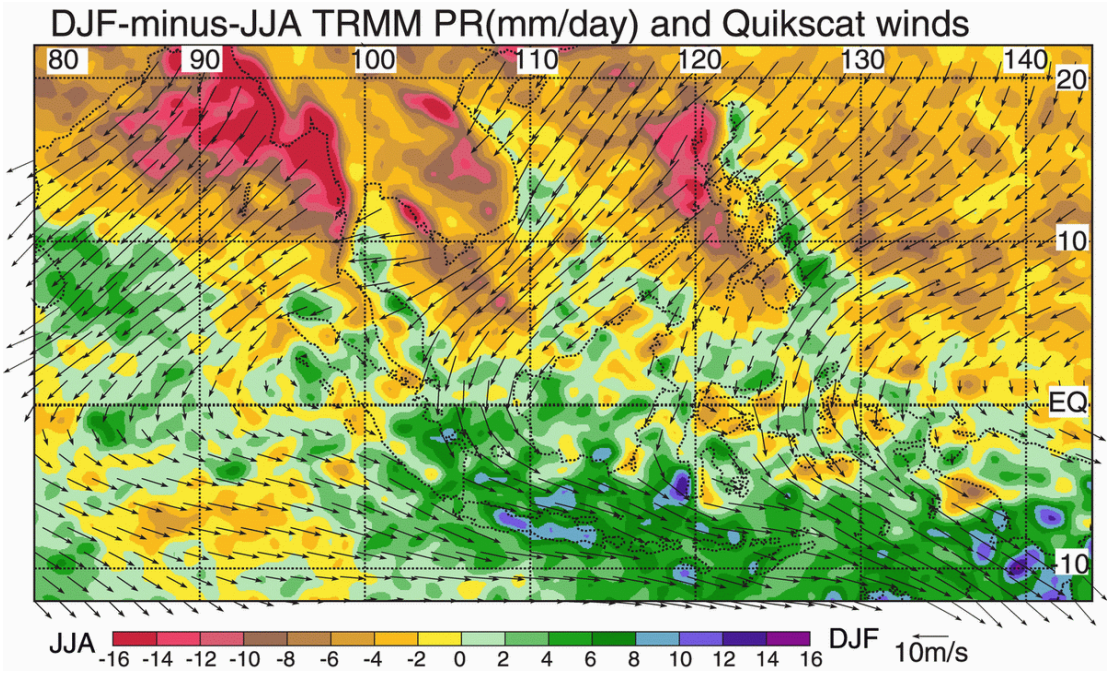

Figure 8. Differences of TRMM PR rainfall and QuikSCAT winds between boreal winter and boreal summer (DJF minus JJA). Warm colors are the boreal summer monsoon regime and cool colors are the boreal winter monsoon regime. (From Chang *et al.* 2004c).

2.4 Regimes of the Transitional Seasons and the Asymmetric Seasonal March

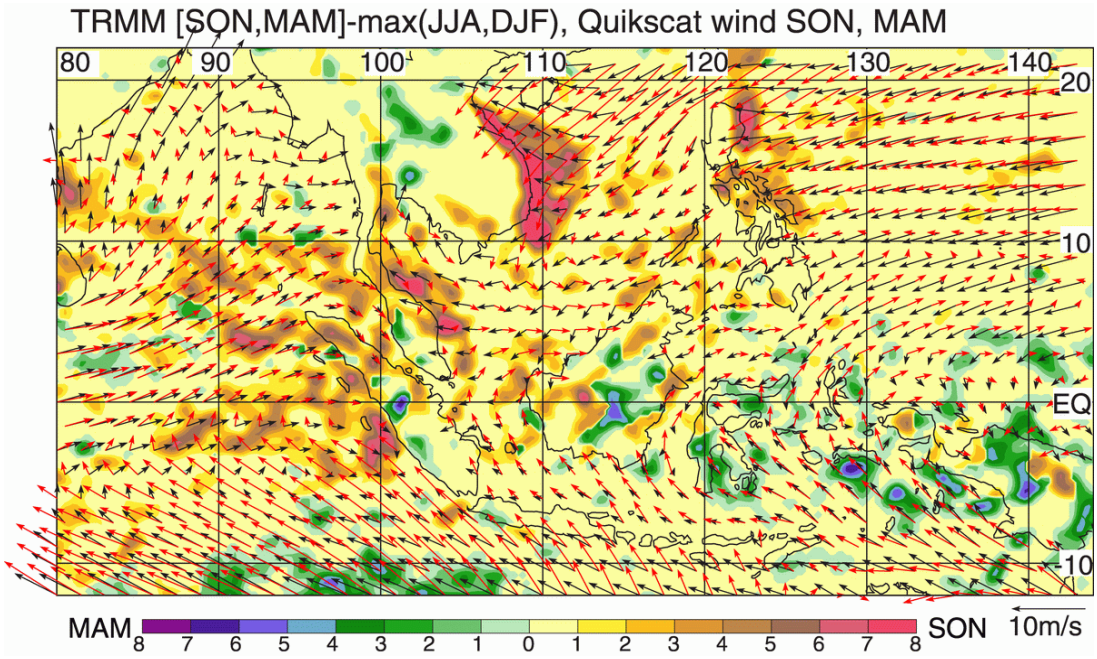

Figure 9. Monsoon regimes during transition seasons deduced form TRMM PR rainfall. A grid point is identified if the rainfall during one of the two transition seasons is the maximum in the annual cycle, and the value plotted is the difference between this transition-season rainfall and the boreal winter and or boreal summer whichever is highest. Warm colors are the boreal fall monsoon regime and cool colors are the boreal spring monsoon regime. The difference of QuikSCAT winds between the two transition seasons (SON minus MAM) is plotted for the entire domain. (From Chang *et al.* 2004c).

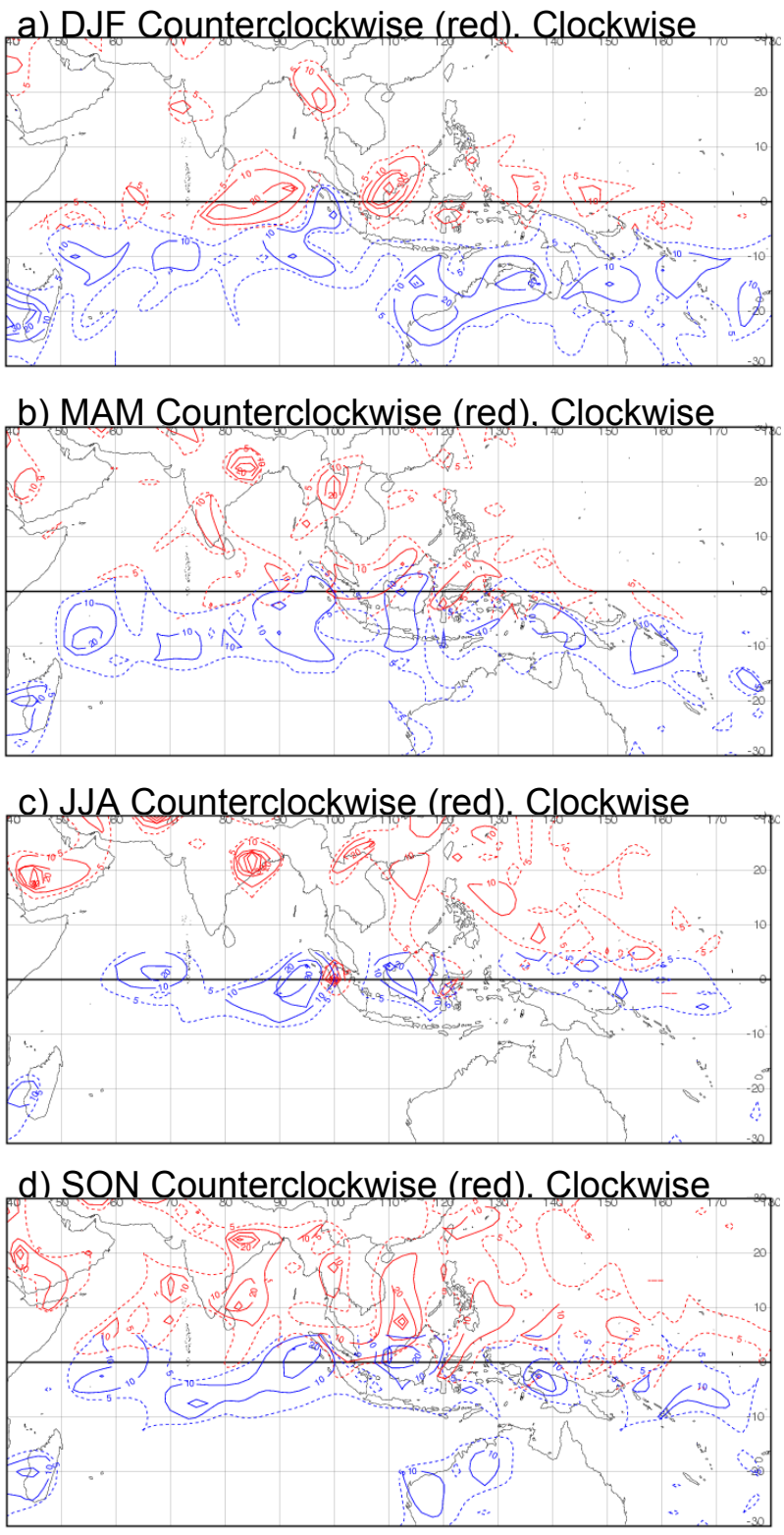

Figure 10. Frequency of 850 hPa closed circulation centers on NCEP/NCAR Reanalysis during August 1997 - December 2002. Red: counterclockwise, Blue: clockwise during boreal a) winter, b) spring, c) summer and d) fall.

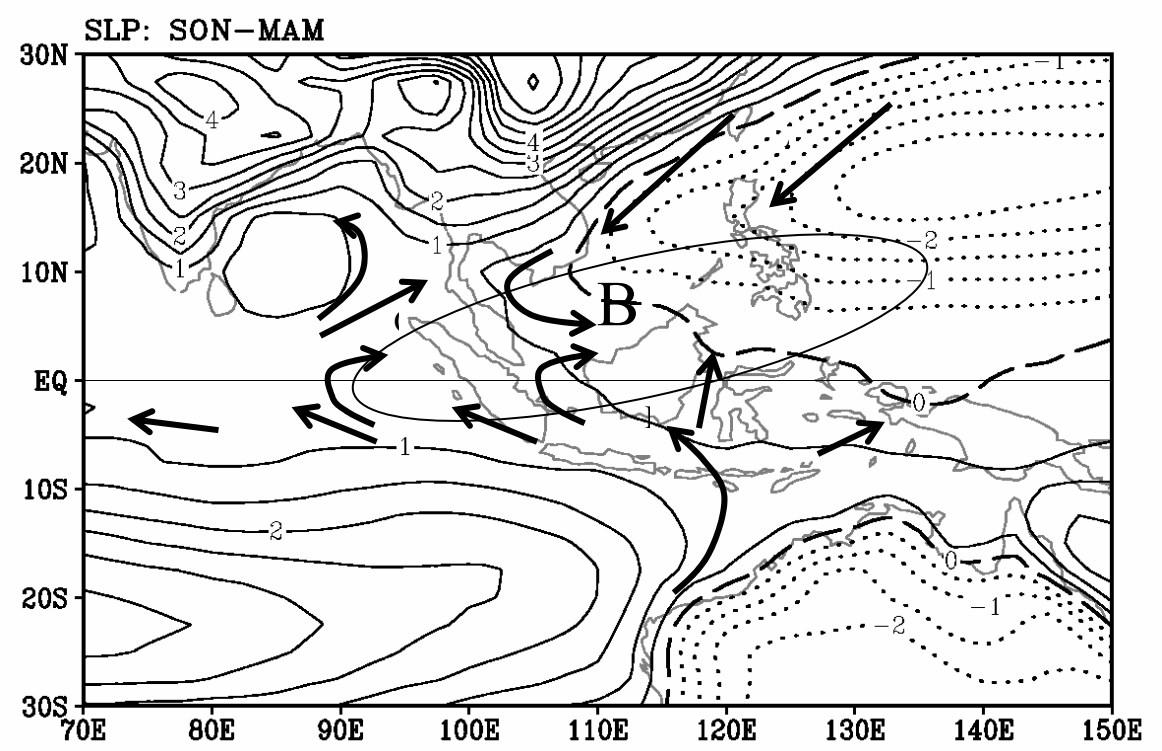

Figure 11. Differences of sea-level pressure between boreal fall and boreal spring (SON minus MAM), unit: hPa. Negative isobars are dotted and the zero line is dashed. Schematics of sea-level wind differences based on the differences in the sea-level pressure pattern are indicated. The elliptic–shaped area indicates preferred belt of convergence in fall and divergence in spring. See text for details. (From Chang *et al.* 2004c).

3. Interannual Variations

3.1. Relationship between Rainfall and ENSO

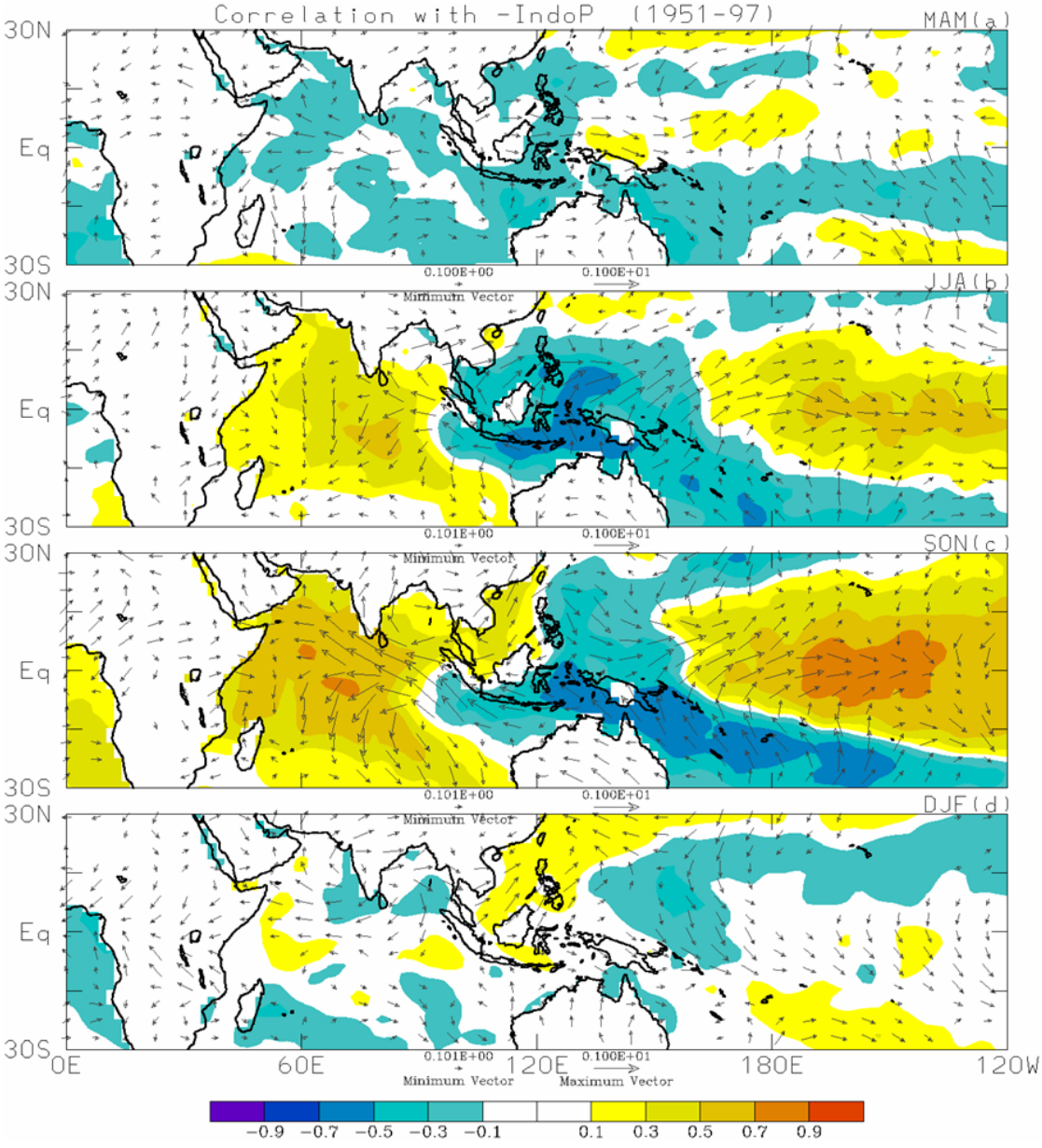

Figure 12. Correlation of monthly mean Indonesian rainfall with Nino34. The long dashed lines indicate significant correlation at the 95% level. (From Hendon 2003)

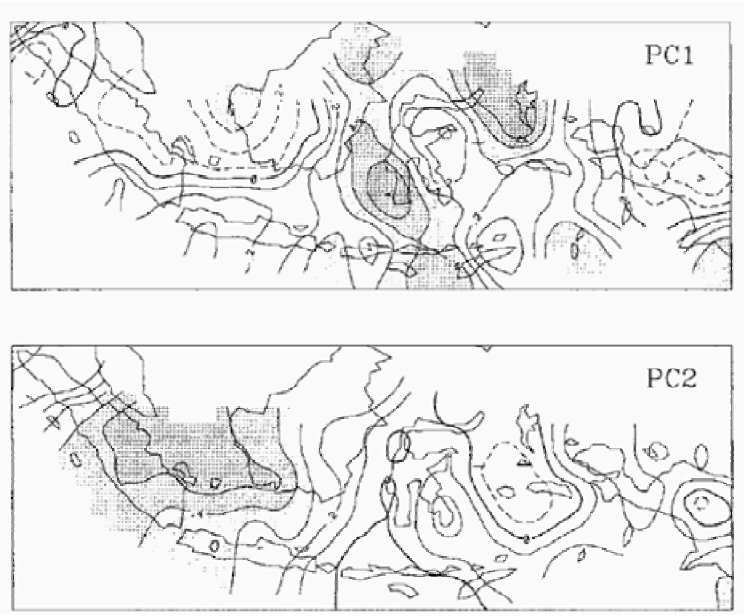

Figure 13. Spatial pattern of loadings of the first two unrotated principal components of DJF rainfall. Contour interval is 0.1, the zero contour is bold, negative contours are dashed, and areas above 10.3 and below 20.3 are shaded. (From Haylock and McBride 2001)

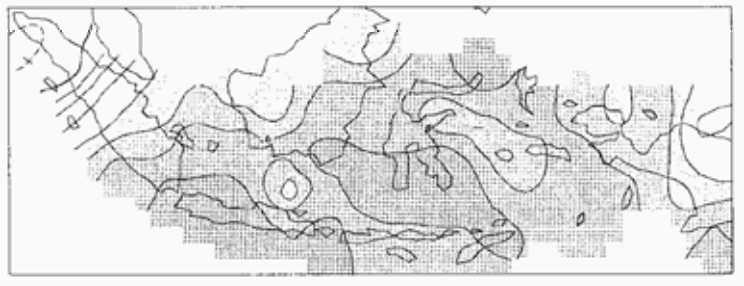

Figure 14. Spatial pattern of loadings of the first unrotated principal component of SON rainfall. Contour interval is 0.1, the zero contour is bold, negative contours are dashed, and areas above 10.3 and below 20.3 are shaded. (From Haylock and McBride 2001)

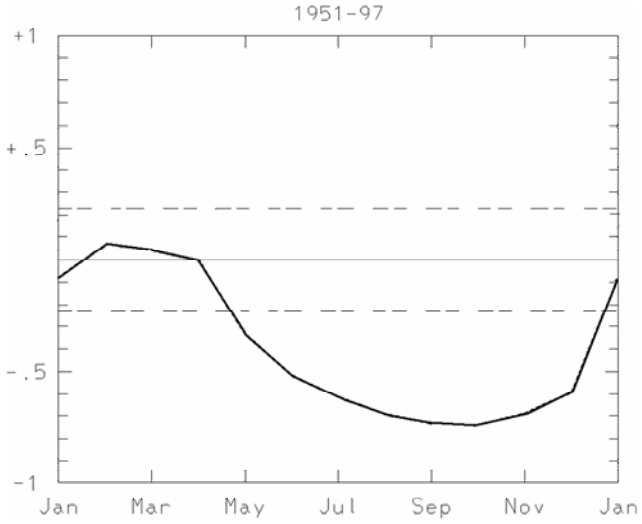

Figure 15. Correlation of seasonal mean Indonesian rainfall with SST (shading) and surface winds (maximum vector is length 1.) for the a) March-April-May, b) June-July-August, c) September-October-November, and d) December-January-February seasons. A correlation of approximately 0.24 is significantly different than zero at the 95% confidence level, assuming 46 degrees of freedom. (From Hendon 2003)

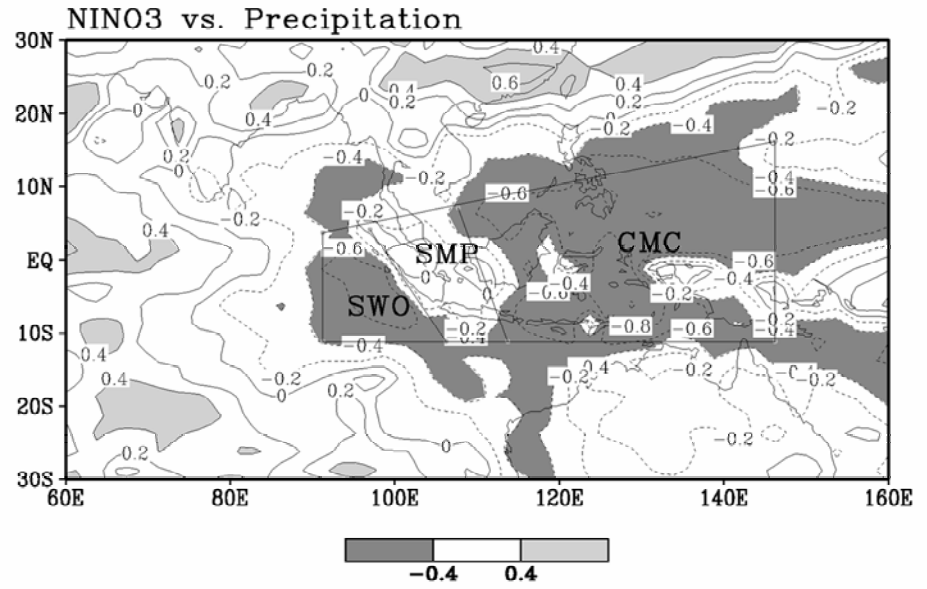

Figure 16. Correlations of 1979-2002 CMAP rainfall with Nino3 SST. Areas above the 5% significance level are shaded. The following rainfall index regions are delineated: SMP: Sumatra-Malay Peninsula; SWO: Southwest oceanic area southwest of Sumatra; and CMC: Central Maritime Continent. (From Chang *et al.* 2004b)

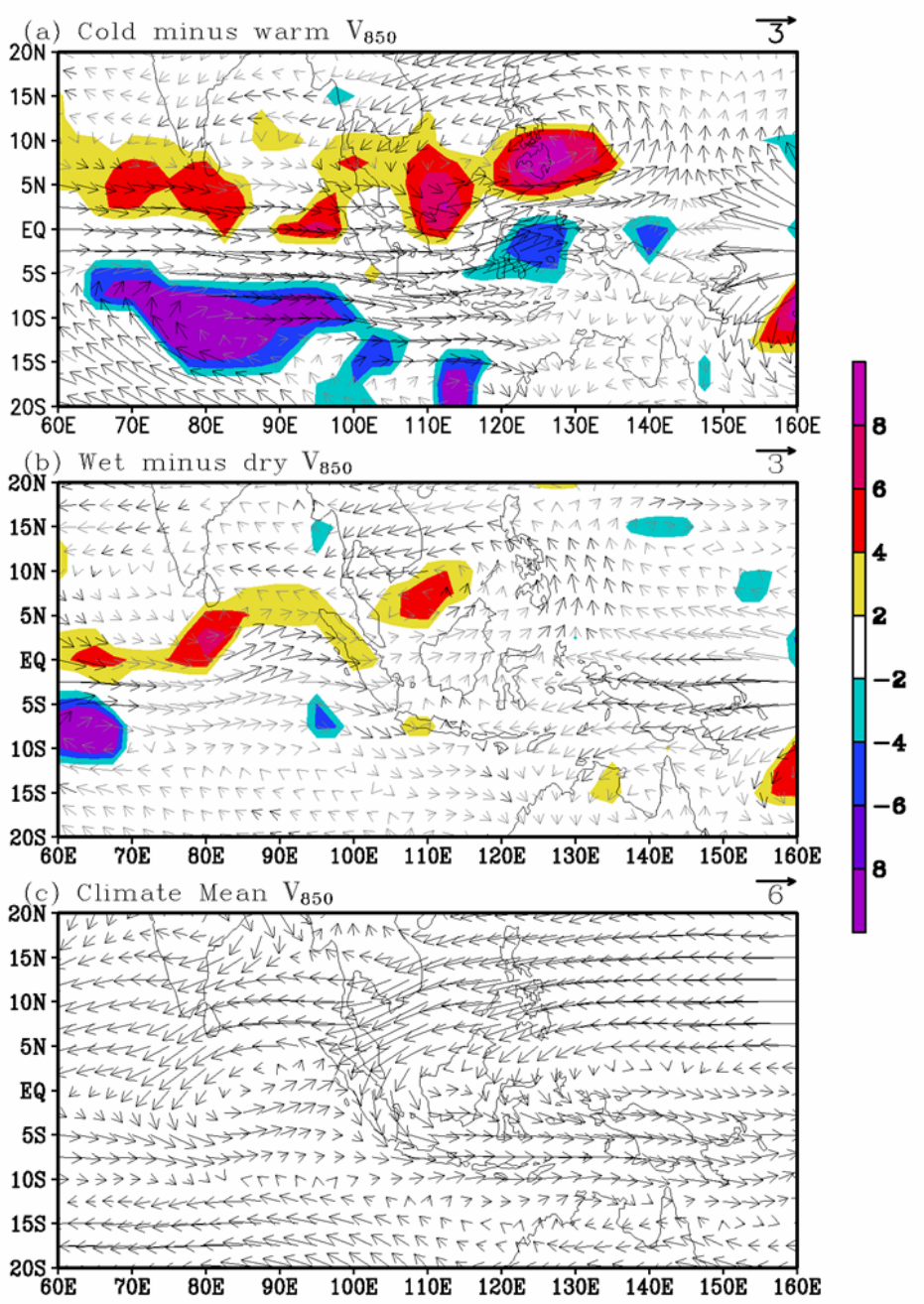

Figure 17. (a) Composite of Nino3 SST "cold minus warm" 850 hPa wind (heavy arrows indicate differences with at least a 95% confidence level in either the zonal or the meridional component) and vorticity (10^{-6} s^{-1}, only differences at 95% or higher confidence level are plotted) during 1979-2002, (b) Same as (a) except for "wet minus dry" in the SMP rainfall index. (c) Long-term seasonal (DJF) mean 850 hPa wind. (From Chang *et al.* 2004b)

3. 2. Interdecadal Variation of Indonesian Rainfall – ENSO Relationship

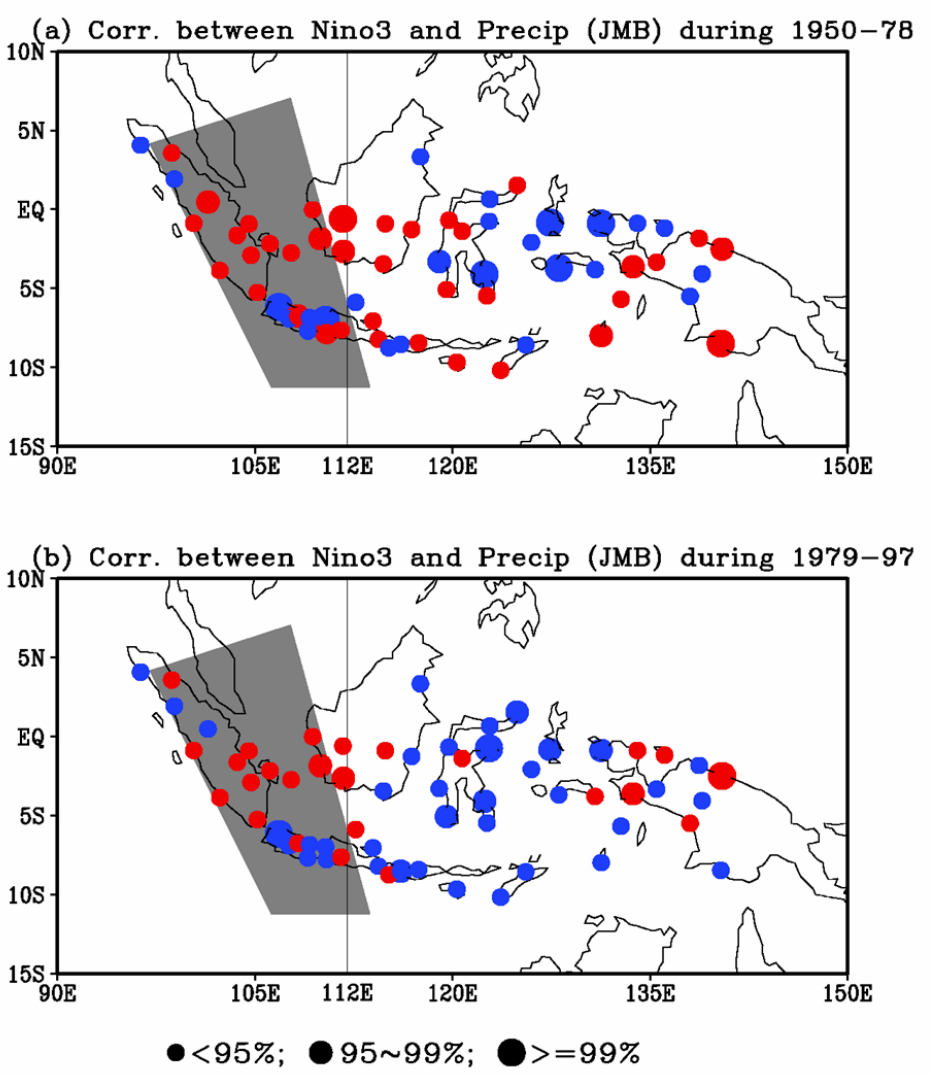

Figure 18. Correlations of Indonesian station rainfall data with Nino3 SST for (a) 1950-78, and (b) 1979-97. Positive (negative) correlations are indicated by red (blue) circles. The sizes of the circles indicate the significant levels: small: below 95%; medium: between 95% - 99%; large: above 99%. The SMP region used in the analysis of CMAP rainfall is shaded. (From Chang *et al.* 2004b)

Table 1. Correlation between Nino3 SST and area-averaged Indonesian station rainfall for western Indonesia (west of 112°E), eastern Indonesia (east of 112°E), and all Indonesia. Values above the 1% significance are in italic bold. The significance of all other values is below the 7.5% level. (From Chang *et al.* 2004b)

Winter (DJF)	1950-78	1979-97	1950-97
Western Indonesia	***0.49***	0.26	0.22
Eastern Indonesia	-0.25	***-0.62***	***-0.44***
All Indonesia	0.16	-0.30	-0.17

3.3 Biennial Oscillations

4. Boreal Winter Convection and Synoptic and Intraseasonal Variations

4.1 Boreal Winter Convection

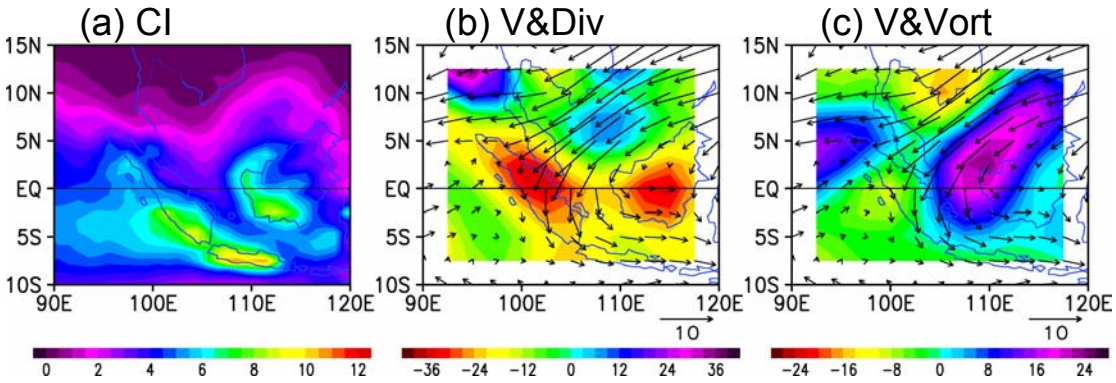

Figure 19. December-February (1979/80-2000/01) mean fields of (a) convective index, (b) 925 hPa winds (m s^{-1}) and divergence (shaded, 10^{-5} s^{-1}), and (c) 925 hPa winds (m s^{-1}) and vorticity (shaded, 10^{-5} s^{-1}). (From Chang *et al.* 2004a).

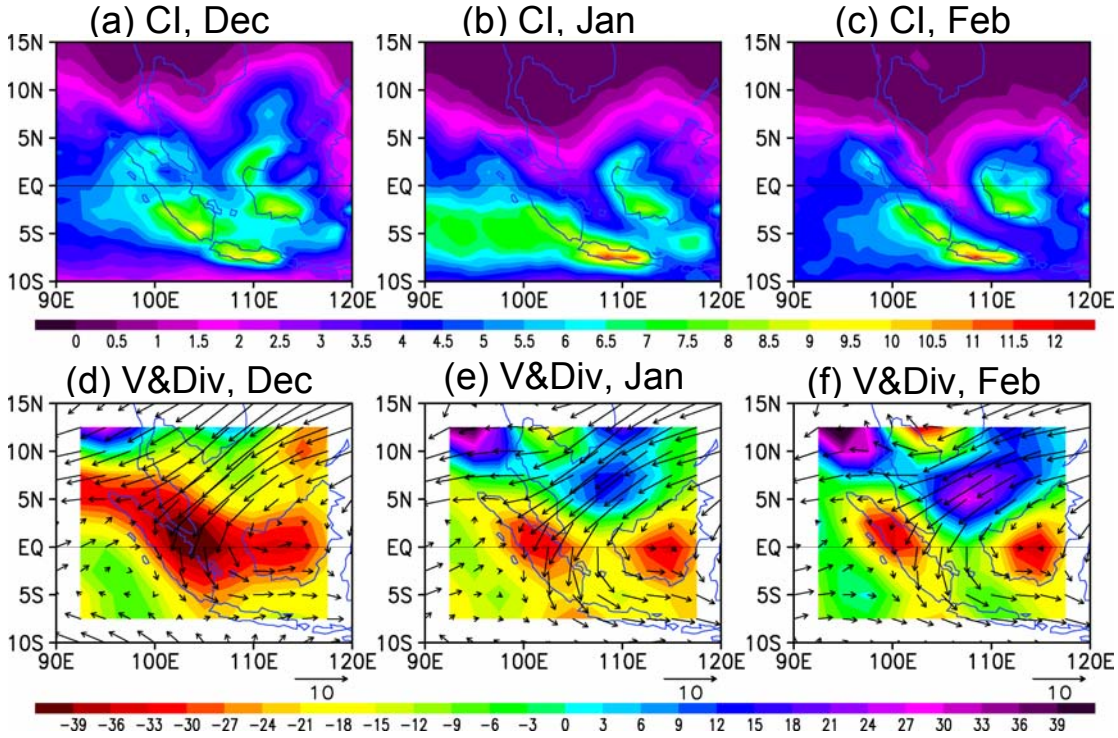

Figure 20. Individual monthly means (1979/80-2000/01) for (top row) convective index and (bottom row) 925 hPa winds (m s^{-1}) and divergence (shaded, 10^{-5} s^{-1}) for (left column) December, (middle column) January, and (right column) February. (From Chang *et al.* 2004a).

4.2. Synoptic-Scale Circulations

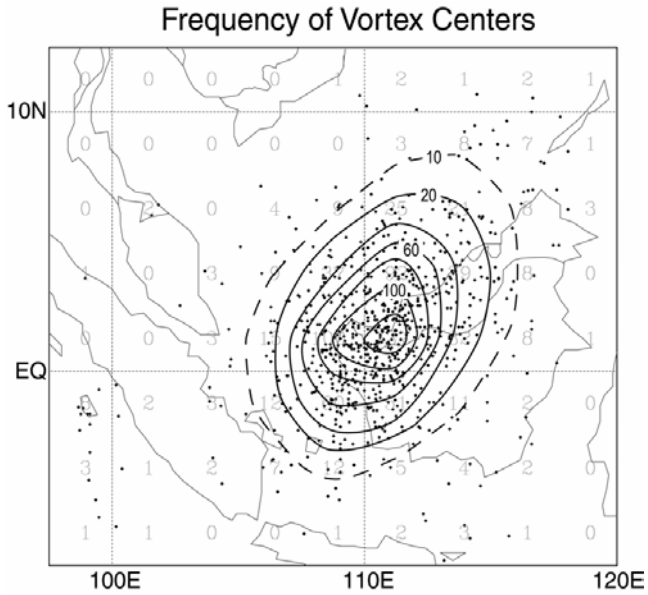

Figure 21. Analyzed Borneo vortex center locations based on streamlines of unfiltered 925 hPa winds. (From Chang *et al.* 2004a).

Table 2. The distribution of Borneo vortex days with respect to the presence of a surge or no surge.

	No-Vortex Days	Vortex Days
No-Surge Days	1038	477
Surge Days	229	151

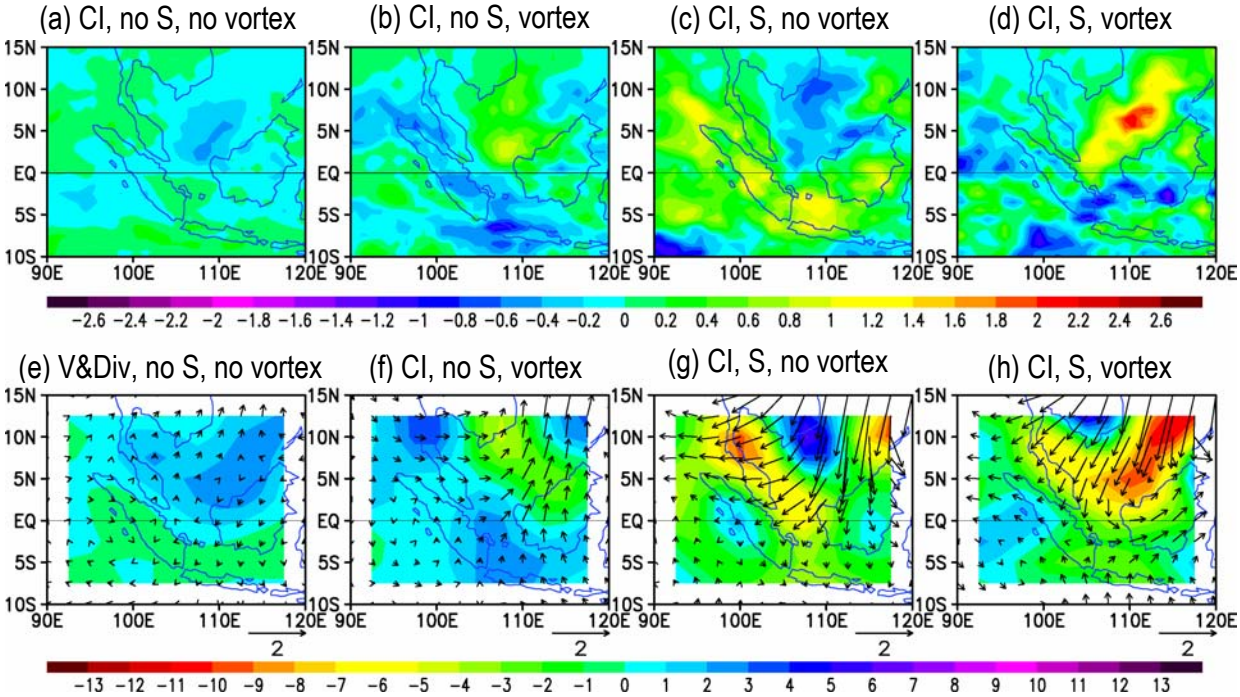

Figure 22. Composite maps of (top row) convective index and (bottom row) 925 hPa winds (m s^{-1}) and divergence (shaded 10^{-5} s^{-1}) for (a,e) no surge and no vortex cases, (b,f) no surge and vortex cases, (c,g) surge and no vortex cases, And (d,h) surge and vortex cases. (From Chang *et al.* 2004a).

4.3 Madden-Julian Oscillation

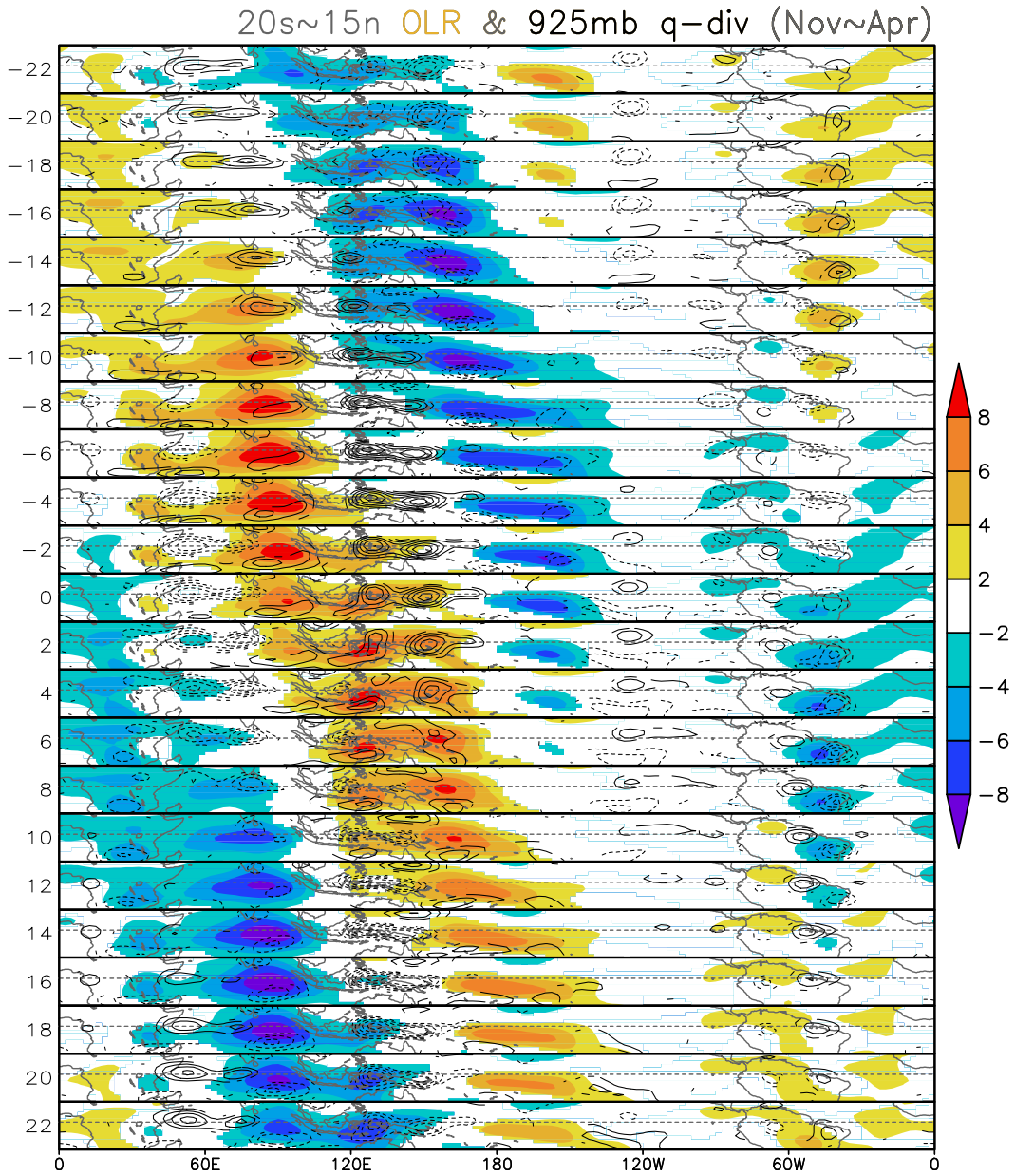

Figure 23. The spatial distribution of intraseasonal OLR and low-level divergence composite for 22 days before and 22 days after the time that the convection maximum proceeds across the Maritime Continent, which is defined as day 0. The horizontal dashed line indicates the equator. (From Hsu and Lee 2004)

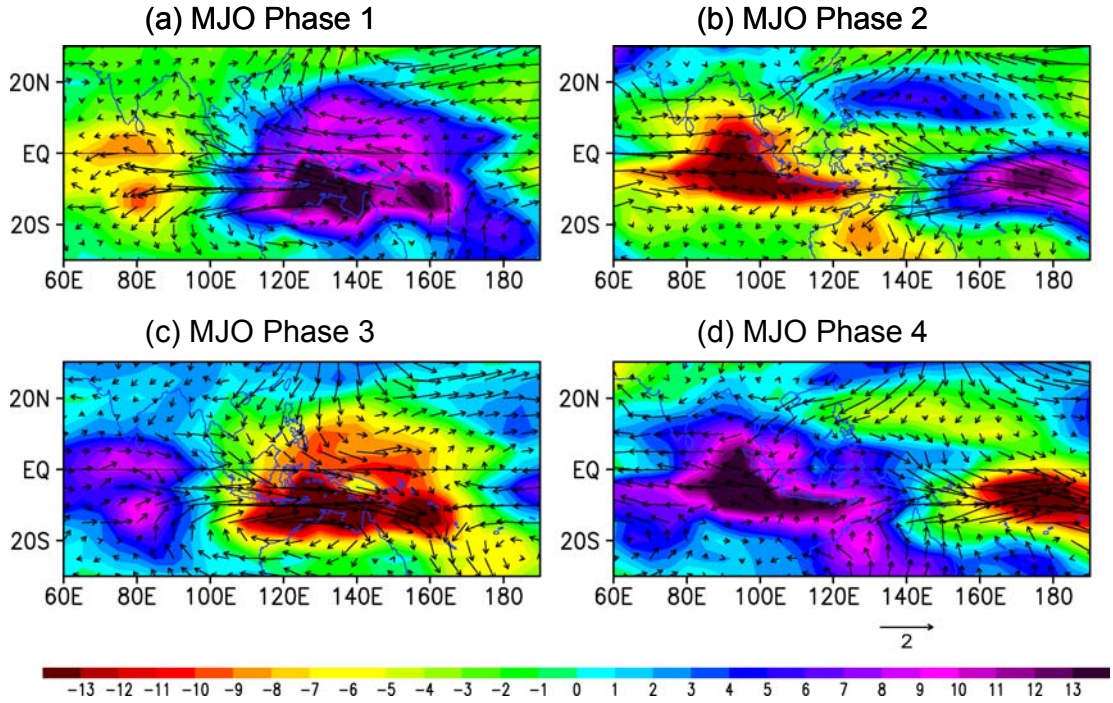

Figure 24. Composite 850 hPa winds (m s^{-1}) and anomalous outgoing longwave radiation (OLR), W m^{-2}) for the four phases of the MJO based on time coefficients of an SVD analysis of the winds and OLR. (From Chang *et al.* 2004a).

Table 3. The number of surge cases with respect to the MJO and phase of the MJO.

	No-MJO Days	MJO Days	MJO Phases 1-2	MJO Phases 3-4
Number of No-Surge Days	845	670	381	289
Number of Surge Days	242	138	56	82
Percentage of Surge Days	29%	21%	15%	28%

Table 4. The distribution of vortex cases (days) with respect to MJO periods and phases.

	No MJO	MJO			
No-Vortex	675	542			
		Phase 1	Phase 2	Phase 3	Phase 4
		148	163	157	124
Vortex	412	216			
		Phase 1	Phase 2	Phase 3	Phase 4
		57	69	50	40

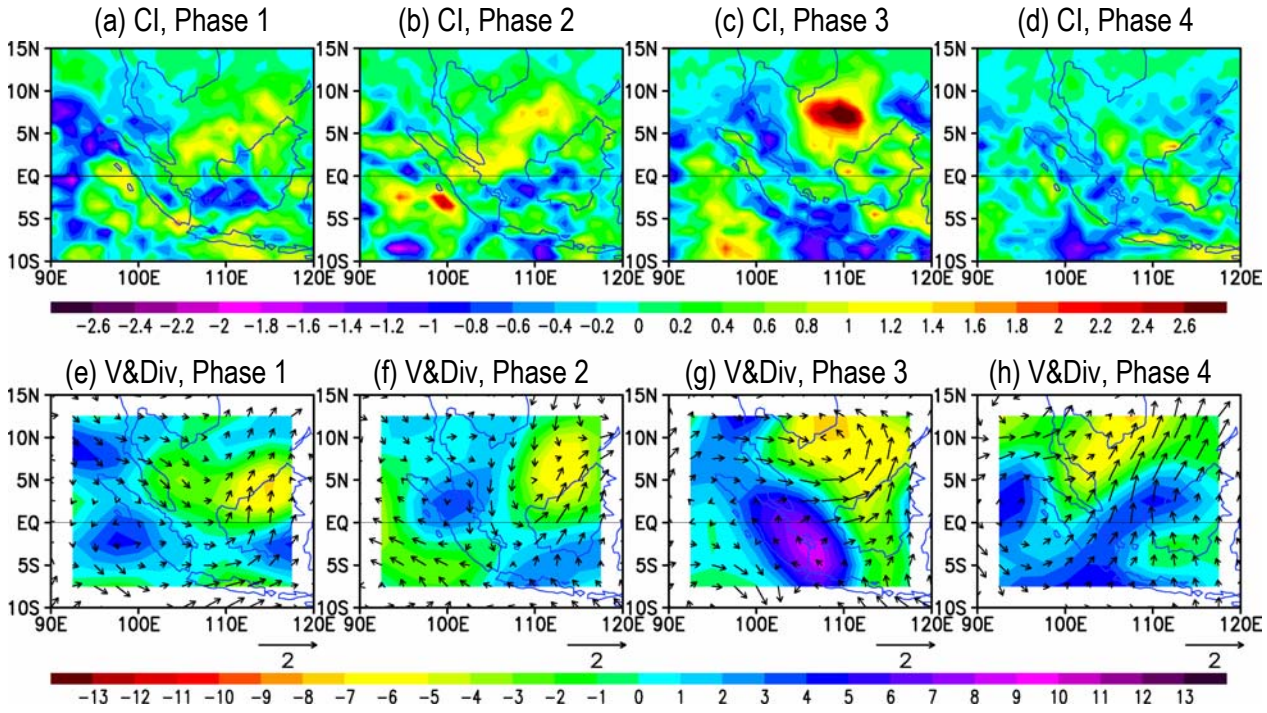

Figure 25. Composite maps of (top row) convective index and (bottom row) 925 hPa winds (m s^{-1}) and divergence (shaded, 10^{-5} s^{-1}) for MJO and vortex cases when the MJO is in (a,e) Phase 1, (b,f) Phase 2, (c,g) Phase 3, and (d,h) Phase 4. The MJO phases are as defined in Fig. 19. The number of cases in each composite is defined in the bottom row of Table 4. (From Chang *et al.* 2004a).

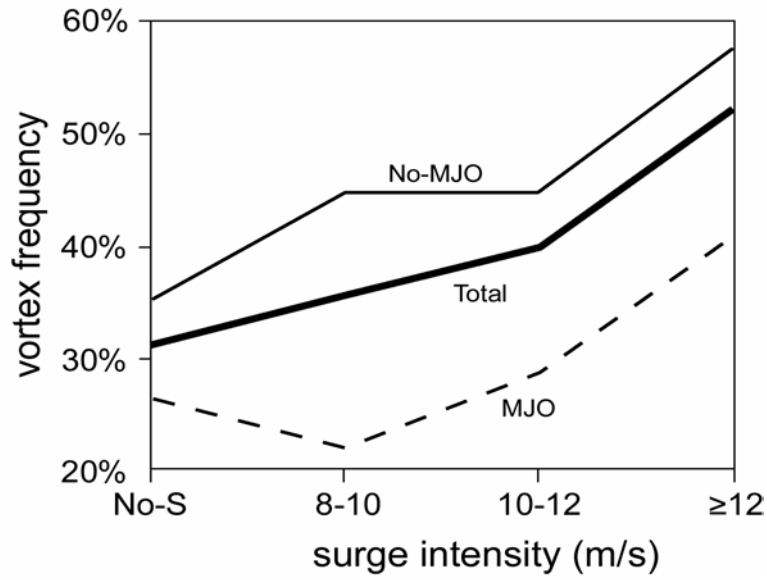

Figure 26. Summary of the percentage of days with no surge (No-S), weak surge (8-10), moderate surge (10-12), and strong surge (≥12) that also contain a vortex for all days, no-MJO days, and MJO days.

THE AUSTRALIAN SUMMER MONSOON

HARRY HENDON

Bureau of Meteorology Research Centre
Melbourne 3001, Australia
E-mail: hhh@bom.gov.au

(With contributions from Matthew Wheeler and John McBride, BMRC)

1. Introduction

The Australian summer monsoon is traditionally referred to as the wet season in Northern Australia when over three-quarters of the annual rainfall occurs. The circulation during the monsoon is characterized by lower tropospheric westerlies to the north of a monsoon trough (Fig. 1 from Hung *et al.* 2004), overlain by a broad region of upper tropospheric easterlies (e.g., Troup 1961). The Australian summer monsoon is just a portion of the greater Indonesian-Australian Monsoon that extends from the equator to about 15S and westward from 100E to about 155E. Here we touch on aspects of the onset process, the role of the MJO for intraseasonal and interannual variability, and the impact of ENSO

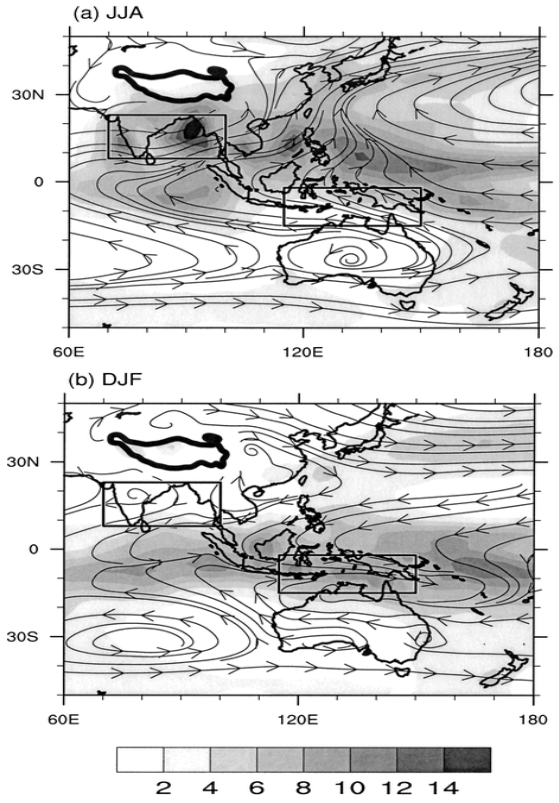

Figure 1 Mean streamlines at 850mb (contours) and precipitation (shaded, mm/day) for JJA and DJF. From Hung et al. 2004

2. Broadscale Evolution

The Australian monsoon ultimately results from sensible heating over the continent that leads to a reversal of the lower tropospheric meridional temperature gradient (warmer over land to the south than over the ocean to the north). A thermally induced meridional circulation then develops (i.e., a giant sea breeze; e.g., Hung and Yanai 2004). Low level onshore north-westerlies transport moist air inland, which allows the monsoon to expand poleward over arid northern Australia. In conjunction with development of the monsoon trough, lower tropospheric westerlies and associated widespread rainfall replace the dry-trade easterlies that predominate during winter. Onset of the monsoon, typically in late December, also coincides with a rapid poleward contraction of the subtropical jet and ridge (Fig. 2, from Hendon and Liebmann 1990a). After onset the trade easterlies strengthen south of the trough and upper tropospheric easterlies develop, yielding a tropical circulation with a deep baroclinic structure. Along about 10–15°S a line of strong cyclonic ($-\partial u/\partial y$) shear separates lower latitude westerlies from higher latitude easterlies (McBride and Keenan, 1982). The monsoon typically retreats by April.

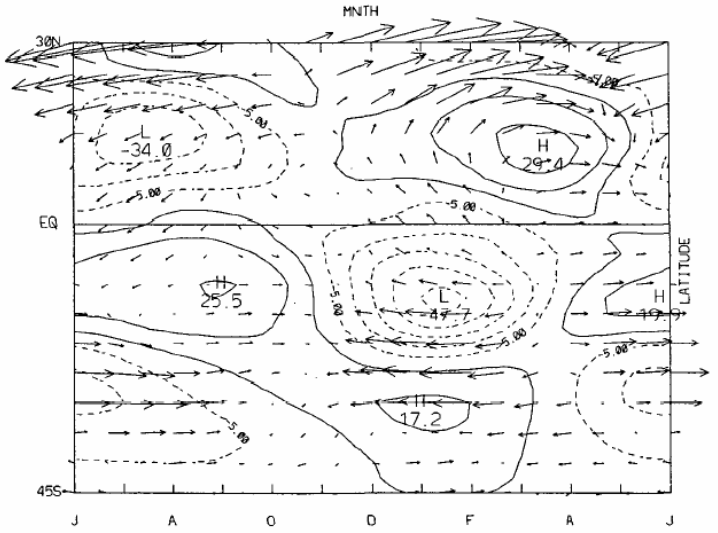

FIG. 2. First three harmonics of the annual cycle (annual, semiannual, terannual) of OLR (contoured) and ECMWF 200 mb winds (vectors) averaged between 130–145 E. Contour interval is 10 W m^{-2} (first contour at ±5 W m^{-2}) and maximum vector wind has magnitude 30 m s^{-1}. See text for details.

Figure 2 First three harmonics of annual cycle of OLR (contour) and 200 mb winds (vectors) averaged in the Australian sector (130-145E). From Hendon and Liebmann 1990.

3. Bursts, Breaks, and Intraseasonal Variability

The monsoon is composed of bursts and breaks that typically last 1-3 weeks (Fig. 3, from Wheeler and McBride 2004). Onset typically coincides with beginning of an active burst. The burst and breaks are often a reflection of passage of the Madden-Julian Oscillation (MJO; e.g., 1987/88). But, the MJO is not the only source of intraseasonal variability nor is it the trigger for every onset.

The role for the MJO in driving monsoon variability is quantified by spectral analysis of zonal at 850 mb at Darwin and northern Australia rainfall (Fig. 4, from Hendon and Liebmann 1990b). A spectral peak in the MJO band (30-70 days) in zonal wind is evident, but not in rainfall. The peak in zonal wind only stands out above the background spectrum (here subjectively determined by averaging across frequencies adjacent to the MJO band) by about a factor of 0.5. That is, the MJO

signal only accounts for about 1/3 of the zonal wind variance in the 30-70 day range. No peak is evident in rainfall, which reflects the much nosier nature of convective rainfall even after spatial averaging. However, rainfall is coherent with zonal wind in the 30-70 day band. Rainfall leads zonal wind by a few days, which is typical of the MJO. Thus, the MJO clearly impacts variability of the monsoon, but usually in only a modest fashion.

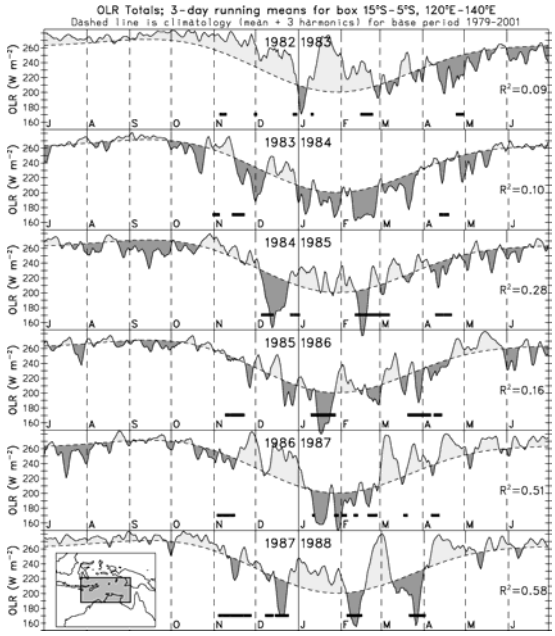

Figure 3 From Wheeler and McBride 2004. OLR averaged to north of Australia (box given in insert). Dashed line s mean seasonal cycle. Heavy bars indicate periods of active convection associated with the MJO, as determined by CEOF analysis of equatorial averaged OLR and zonal wind at 850mb and 200mb. R**2 values are explained OLR variance in the boxed region for each summer monsoon season by the MJO.

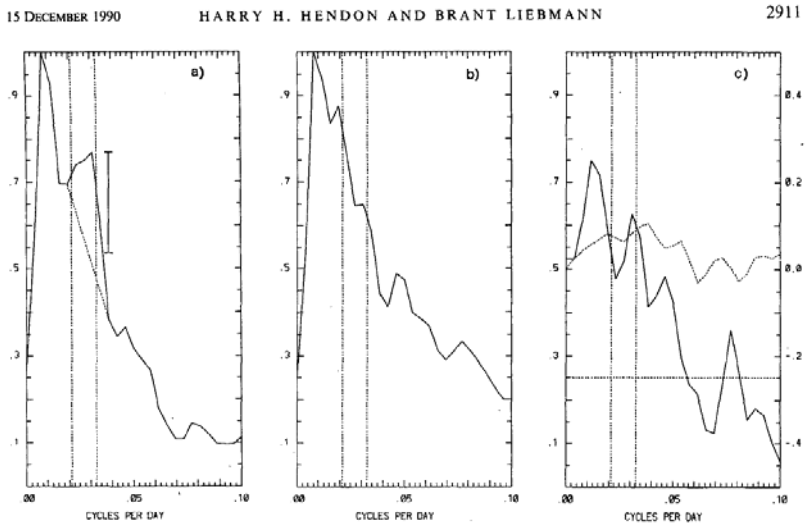

FIG. 2. Power spectra of (a) U_{850} at Darwin and (b) North Australian rainfall for the summer seasons (15 October–15 April) 1957–87. The power has been normalized to unity and only frequencies less than 0.1 cycles per day are shown. The vertical lines demark the "30–50" day period range (frequency band 5.5/256–8.5/256 cpd). The 95% confidence limit (assuming 62 degrees of freedom) for the spectral peak at 32 day period and the bandwidth (1/256 cpd; horizontal bar) are shown in (a). A subjective estimate of the background spectrum in (a) was made by the linear fit between the adjacent spectral minima to the 30–50 day band (dashed line). (c) The coherency squared (solid) and phase (dashed) between U_{850} and North Australian rainfall. The scale for coherency squared is on the left and phase angle (in cycles) is on the right. A positive phase indicates rainfall leads U_{850}. The horizontal line is the 95% confidence limit (assuming 62 degrees of freedom) for the coherency squared estimate.

Figure 4 From Hendon and Liebmann 1990b.

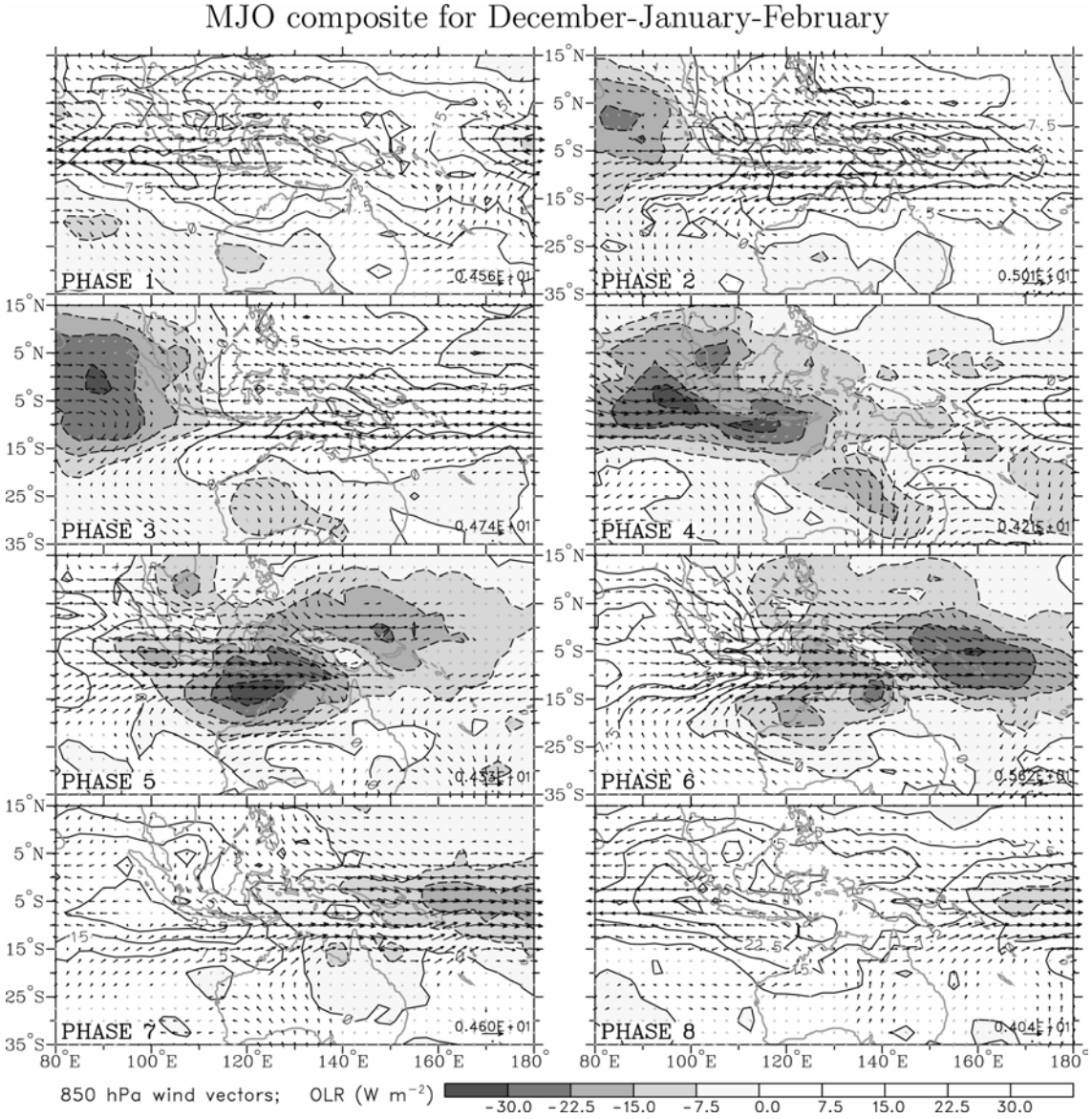

Figure 5: Composited OLR and 850-hPa wind anomalies for eight phases of the MJO during December-January-February (DJF). OLR contour interval is 7.5 W m^{-2}, with negative contours dashed and negative values shaded. Black vectors indicate wind anomalies that are statistically significant at the 99% level, based on their local standard deviation and the Student's t test. Grey vectors do not pass the 99% level test. The magnitude of the largest vector is shown on bottom-right of each panel. From Wheeler and Hendon 2004

While the MJO may only play a modest role in the monsoon when all years are considered together, there are clearly times that the MJO dominates monsoon variability. The role of the MJO in the monsoon is elucidated by objectively identifying the MJO from global analyses and then comparing the monsoon variations to those associated with the broad-scale MJO behavior. Wheeler and Hendon (2004) defined the MJO by combined EOF analysis of equatorial averaged zonal wind at 200 and 850 mb and OLR. A dominant leading pair of modes is associated with the MJO. The typical structure of the MJO in the Australian monsoon is revealed by composites that are based on the phase of the MJO as given by the projection onto these leading two EOFs (Fig. 5, form Wheeler and Hendon 2004). Suppressed conditions exist at phase 1 and 2 (phases are separated by about 1 week),

with anomalous easterlies across and to the north of northern Australia. Active convection commences at phase 4, with monsoonal westerlies becoming established by phase 5. An interesting tropical-extratropical teleconnection is evident in southwestern Australia at Phase 3, whereby enhanced convection there occurs ahead of the low-level cyclone before convection becoming established to the north at Phase 4. By Phase 7, the active convection has moved off to the east. At Phase 8 the monsoonal westerlies have decayed and suppressed conditions are reestablished. This entire cycle takes on the order of 30-50 days.

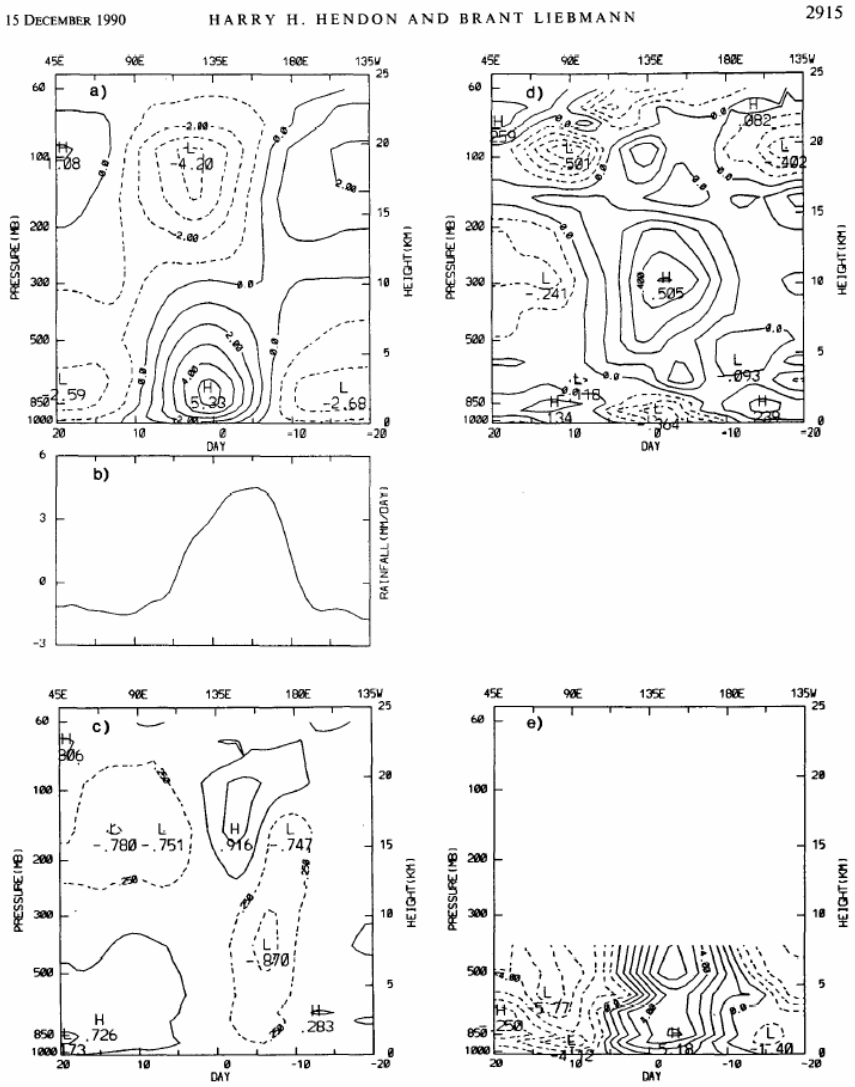

FIG. 5. Composite 30–50 day oscillation (91 events) at Darwin of (a) zonal wind, (b) rainfall, (c) meridional wind, (d) temperature, and (e) relative humidity. Unfiltered fields were composited. The contour intervals are (a) 1 m s^{-1}, (c) 0.5 m s^{-1} (first contour at ±0.25 m s^{-1}), (d) 0.1°K, and (e) 1.0%. Composites run from −20 days to +20 days with day zero corresponding to the maximum 850 mb westerly wind. Note time runs from right to left. The longitudinal scale across the top of the figures is an approximate one assuming that the composited oscillation moves steadily eastward at 4 m s^{-1}. The height scale was approximated hydrostatically from the pressure levels using a constant scale height of 8.5 km.

Figure 6 From Hendon and Liebmann 1990b

Locally at Darwin, the amplitude of the oscillation at Darwin is about 5 ms-1 in zonal wind, 0.75 ms-1 in meridional wind, 5 mm rainfall per day, and 10% in relative humidity (Fig. 6 from Hendon and Liebmann 1990b). The deep baroclinic structure in zonal wind has its node at about 300 hPa. The temperature structure is similar to that described by McBride and Frank (1999), with a warm anomaly of the order of 0.9 K in the upper troposphere and a cold anomaly of similar size in the lower

troposphere. It is also interesting to observe enhanced boundary layer relative humidity ~1 week prior to commencement of active convection. This feature, which may result from a slow vertical build up of convection that progressively moistens and expands the boundary layer, may reflect a process critical to setting the period of the MJO and which may be absent in many GCMs.

A concrete measure for the role of the MJO in each years' monsoon is provided by the multiple correlation coefficient squared, R^2, between the 3-day running-mean OLR anomaly across northern Australia and the projection coefficients onto Wheeler and Hendon's leading pair of EOFS (values indicated in middle right of each panel in Fig. 3). Nearly 60% of the OLR convective variability in the 1987/88 monsoon can be accounted for by the MJO, while in 1982/83 this drops to less than 10%. Some of this interannual variability is likely related to interannual variability in the strength of the MJO itself (e.g., Hendon *et al.* 1999). That is, the variability in the monsoon that is accounted for by the MJO is proportional to the tropically averaged level of MJO activity.

Monsoon variability is also associated with large-scale westward propagating disturbances (McBride 1983; Davidson *et al.* 1983; Keenan and Brody 1988; Hendon *et al.* 1989). Although it can be quite varied, the phase speed of the westward convective envelopes is often about the same, except in the opposite direction, as that of the eastward MJO (~5 m s^{-1}). Usually the westward envelopes are maximized off the equator, and can be accompanied by large variations in the rotational wind as well. Such characteristics are suggestive of an influence on the monsoon by equatorial Rossby (ER) waves (e.g., Matsuno 1966). The structure and evolution of the typical ER wave in the Australian region is displayed in Fig. 7 (from Wheeler *et al.* 2000). The symmetric circulation cells on either side of the equator are clearly seen, though in individual cases symmetry is hard to detect.

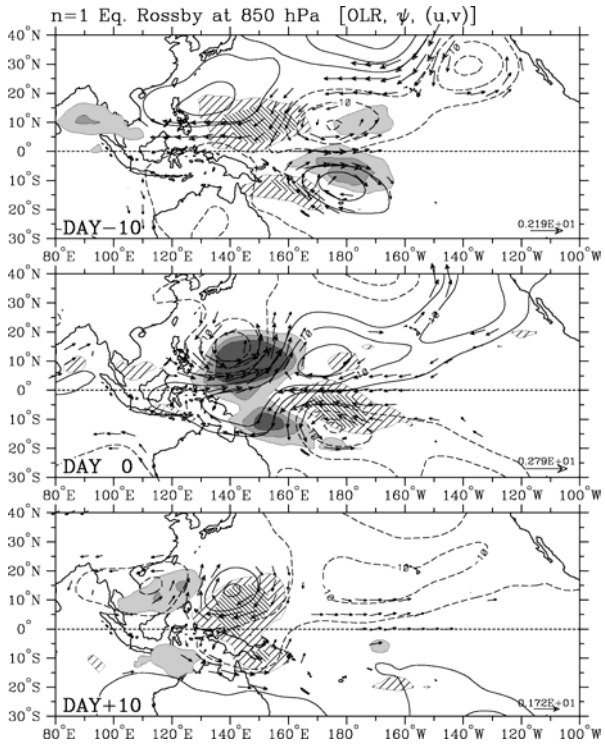

Figure 7: Horizontal structure of a *n*=1 equatorial Rossby (ER) wave over a sequence spanning 21 days, as computed using lagged regression based on a two standard deviation anomaly in the ER wave filtered OLR series at 10°S, 150°E. Shading/cross-hatching show the negative/positive OLR anomalies at the levels of -15, -10, -5, 5, and 10 W m^{-2}. Contours are streamfunction at the 850 hPa level (interval of 5×10^5 m^2 s^{-1}), with negative contours dashed and the zero contour omitted. Vectors are the 850-Pa wind anomalies, plotted only where the local correlation of either wind component is statistically significant at the 99% level. [Reproduced from Wheeler et al. (2000).]

Such westward propagating ER waves were evident during the 1986/87 monsoon. Hovmoller plots of zonal and meridional wind at 850 mb are displayed in Figs. 8 and 9. The waves are detectable as far east as the date line. Also indicated in these figures are the tracks of the tropical cyclones that developed, which are located in the troughs of these disturbances in both hemispheres. As will be discussed in the next section, onset of the monsoon this year also seems to be triggered by arrival of one of these troughs.

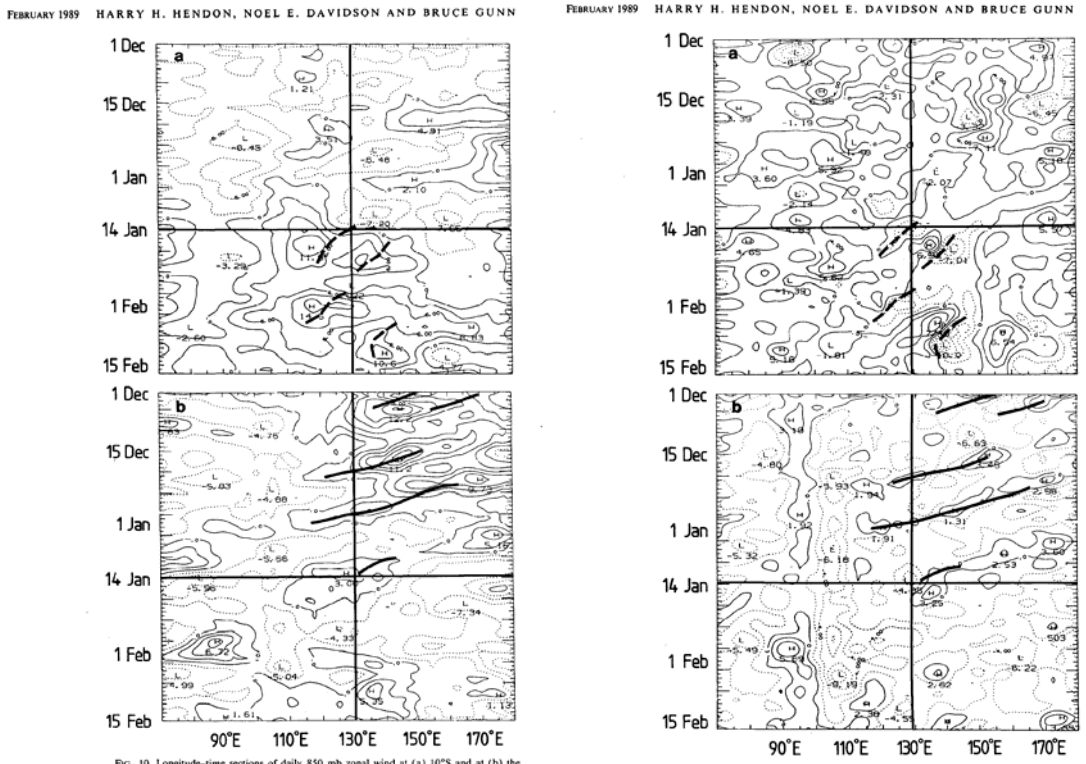

FIG. 10. Longitude–time sections of daily 850 mb zonal wind at (a) 10°S and at (b) the equator. Contour interval in (a) is 3 m s^{-1} and in (b) 2 m s^{-1}. Solid horizontal and vertical lines indicate the approximate location of the AMEX region (130°E and date of onset 14 January 1987). Heavy dashed lines are southern hemisphere cyclone tracks (between 7° and 15°S) while heavy solid lines are for Northern Hemisphere cyclones.

FIG. 11. As in Fig. 10 except for 850 mb meridional wind at 10°S (a) and at the equator (b). The contour interval is 2 m s^{-1}.

Figure 8 Zonal wind at 850 mb along 10S (top) and Eq (bottom) for 1 Dec 1986 – 15 Feb 1987. Heavy dashed (solid curves) are southern (northern) hemisphere cyclone tracks. Heavy horizontal line indicates onset date at Darwin (heavy vertical line) From Hendon and Liebmann (1990)

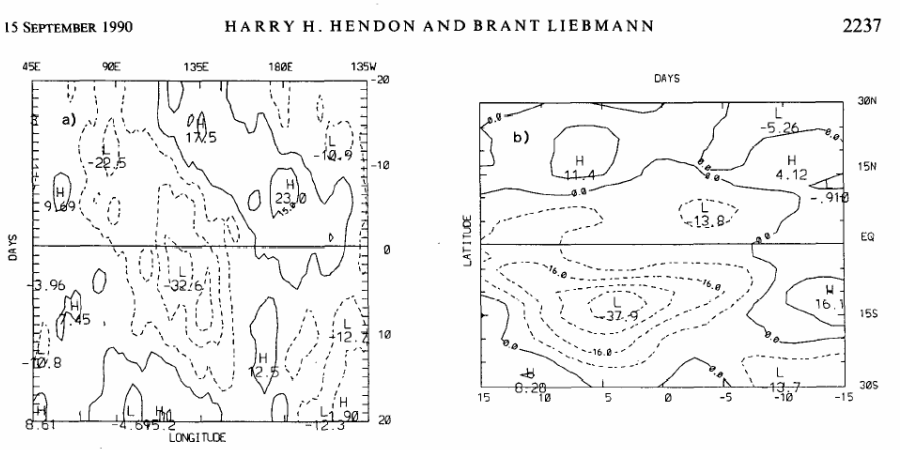

FIG. 12. Composite OLR displayed as (a) Hovmöller diagram averaged between 5°S and 15°S and (b) as latitude versus time averaged between 130°E and 145°E. The contour interval is 10 W m^{-2} in (a) and 8 W m^{-2} in (b). The first contour is at ±5 W m^{-2} in a) and at 0 W m^{-2} in (b). Day zero refers to onset at Darwin. Note time runs down in a) and from right to left in (b).

Figure 9 As in Fig. 8 except for meridional wind at 850 mb

Another potential source of variability within the monsoon is the cross-equatorial influence of cold surges in the South China Sea. These surges are characterized by periods (order several days) of strong cross-equatorial northerly winds, anomalously low temperatures, and an increase in surface pressure in the South China Sea. Compo *et al.* (1999) found submonthly (6–30 day) time-scale surges were directly related to convective activity south of Indonesia. Sumathipala and Murakami (1988), on the other hand, found no contribution of lower-frequency, 30–60 day, northerly surges of east-Asian origin to convection in the Australian-Indonesian monsoon. Instead, they found a contribution from northeasterly flows originating in the subtropical north Pacific.

4. Thermodynamic Changes and Triggers of Onset

From a local thermodynamic perspective, onset involves a gradual built up of low level moist static energy and CAPE, but with significant convective inhibition. For example, in November and December 1986 pre monsoon conditions existed (Fig. 10, from Hendon *et al.* 1989), with large CAPE and strong mid-troposphere static energy minimum but dry boundary layer. The build up of low-level moist static energy and CAPE results primarily from an increase in surface temperature. CAPE is not realized prior to onset due to strong convective inhibition from a lack lower tropospheric humidity. That is, parcels would have to be lifted more than 100 mb from the surface to become buoyant prior to onset. The AMEX experiment in January 1987 experienced an active monsoon. Widespread, deep convection increased mid tropospheric temperature, decreased lower tropospheric temperature and reduced CAPE. But, the increase in low level humidity also lead to dramatically reduced convective inhibition. McBride and Frank (1999) describe a similar contrast between active and break episodes of the monsoon.

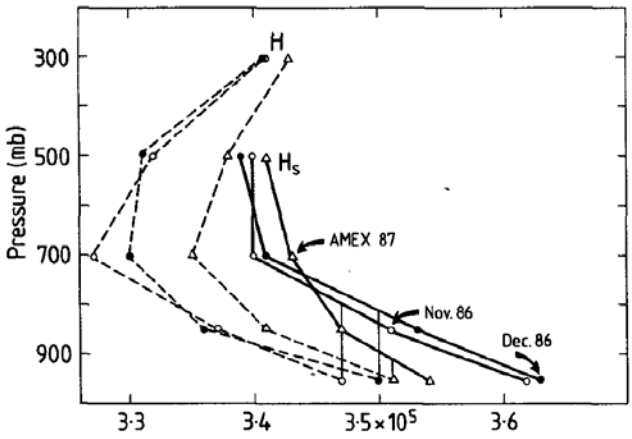

FIG. 6. Thirty-day mean vertical profiles of moist static energy, $H = c_pT + Lq + gz$, (dashed line) and saturated moist static energy $H_s = c_pT + Lq_s + gz$ (dotted line) for periods beginning on 15 November, 15 December and 15 January 1987. Grid point data were averaged between 10° and 12.5°S, 130° and 145°E. Vertical lines indicate undilute parcel ascent from 950 mb. Intersection with Hs coincides with level of parcel buoyancy.

Figure 10 From Hendon et al. 1989

These changes in stratification before and after onset are also reflected in the changes in the characteristics of convection. Convection during the premonsoon (and break periods) is less widespread but has higher vertical development, higher reflectivity above the melting level, a lack of large stratiform decks, more intense updrafts, and higher electrical activity (e.g., Keenan and Carbone 1992). In comparison, convection during the active westerly monsoon is widespread with weaker

updrafts and often associated with squall-like structures within large mesoscale stratiform decks (e.g., Keenan and Rutledge 1993). Thus, while active monsoon conditions result in more widespread rain, the individual convective cells involved are generally less intense. To some extent these differences can be attributed to a continental as compared to maritime source of the airstream in which the convection is embedded. The active monsoon tends to have low level flow from the north (onshore), while the premonsoon and break periods experiences flow from the south (off the continent). However, such differences in convective characteristics are also consistent with the general large-scale static stability changes discussed by Hendon et al. (1989) and McBride and Frank (1999).

While the switch from dry, south-easterlies to wet north-westerlies is sudden, sensible heating from the ground surface, which contributes to the creation of the land-sea thermal contrast in the Australian sector, begins as early as September (Hung and Yanai 2004). Hence, some other trigger is required to instigate the sudden onset. Possible candidates include passage of the convective phase of the MJO or other synotic-scale tropical waves that produce moist northweserly flow and lower tropospheric convergence (e.g., Davidson et al. 1983; Hendon et al. 1989) and penetration of extratropical troughs that perhaps act to destabilize the upper troposphere (e.g. Davidson et al. 1983; Hung and Yanai 2004).

A case for the role of the MJO in the onset of the monsoon can be made by compositing daily OLR and other meteorological variables relative to a subjectively defined onset date. Unfortunately, determination of onset date is not unique and subsequent interpretation depends on the definition of onset. Hendon and Liebmann (1990a) defined onset as the first occurrence of broad-scale wet conditions in northern Australia in conjunction with westerly 850 mb winds at Darwin, based on weakly low pass filtered daily data (i.e., periods shorter than 3-4 days were removed). The composite evolution of zonal wind about onset is consistent with that produced by the MJO: onset coincides with development of deep westerlies overlain by upper tropospheric easterlies that persist for about 2-3 weeks. The evolution of OLR for the composite onset (Fig. 11, from Hendon and Liebmann 1990a) reveals that onset is associated with the slow eastward propagation of convection from the Indian Ocean that typifies the MJO. At Australian longitudes, low OLR (enhanced convection) dips southward at onset and then retreats equator as the convective phase passes into the western Pacific. Hendon and Liebmann (1990a) note, however, that the standard deviation of these composite OLR anomalies is as large as the composite itself. Thus, the role of the MJO is not necessarily dominant. By taking a more local view of the monsoon onset (i.e. development of deep westerlies at Darwin), Drosdowsky (1996) made the case that the MJO was no more important than any other synoptic variability.

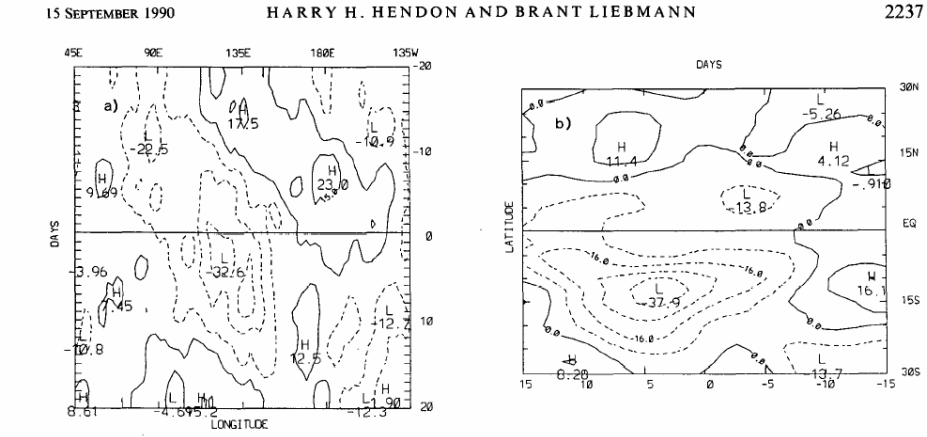

FIG. 12. Composite OLR displayed as (a) Hovmöller diagram averaged between 5°S and 15°S and (b) as latitude versus time averaged between 130°E and 145°E. The contour interval is 10 W m^{-2} in (a) and 8 W m^{-2} in (b). The first contour is at ±5 W m^{-2} in a) and at 0 W m^{-2} in (b). Day zero refers to onset at Darwin. Note time runs down in a) and from right to left in (b).

Figure 11 From Hendon and Liebmann 1990a

Wheeler and Hendon (2004) re-examined the relationship between monsoon onset and the state of the MJO, as defined by the leading pair of EOFs of equatorial averaged zonal wind and OLR (Fig. 12, from Wheeler and Hendon 2004). Onset dates were determined by Drosdowsky (1996). When the MJO is strong, onset occurs more than 80% of the time when the MJO is in Phases 4–7 (i.e., when MJO low-level westerlies and broad-scale convection are in the vicinity of northern Australia) and less than 20% of the time in all the other phases (i.e., when northern Australia is in the suppressed phase of the MJO). The spread of onsets from Phases 4 to 7 covers a time window of half the period of the MJO (i.e., about 20 to 30 days), which is significantly greater spread than the ±4 days found by Hendon and Liebmann (1990a). However, Hendon and Liebmann used a "local" definition of the MJO (i.e. low pass filtered (periods shorter than about 3 days removed) winds and rainfall in the Australian sector), which clearly captures variability besides that due to the MJO. Thus, it appears that the MJO limits monsoon onset to within its active half-cycle, but the actual onset is often set by other, presumably shorter time-scale, phenomena. This view is consistent with Hung and Yanai (2004) and the earlier study of Hendon *et al.* (1989), both of who found the large-scale, low-frequency, influence of the MJO to be only one of a number of factors that determine onset.

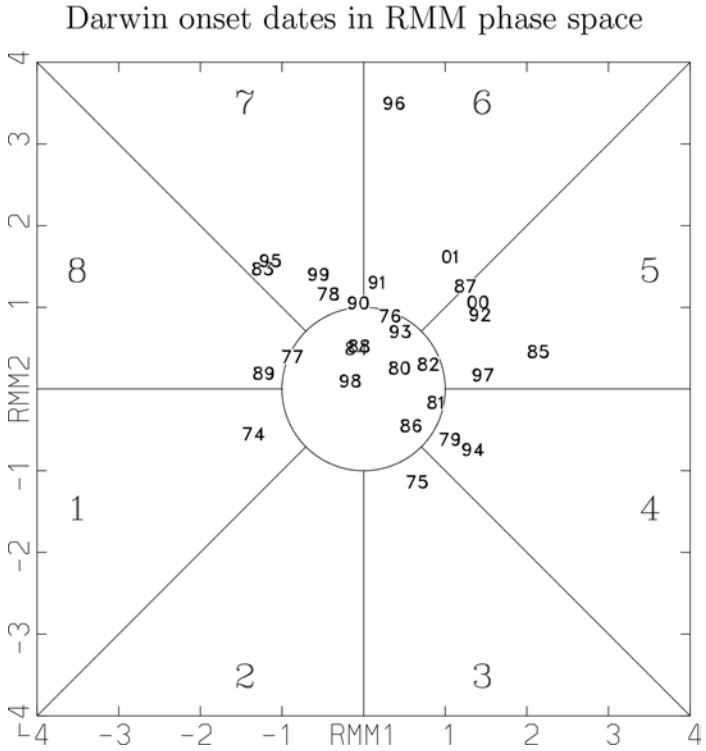

Figure 12: Onset date each year as a function of the state of the MJO, given by the projection onto the leading CEOFs of equatorially averaged OLR, and zonal wind at 200 and 850 mb. Onset dates are based on the daily deep-layer mean zonal wind, at Darwin, Australia as given by Drosdowsky (1996). Reproduced from Wheeler and Hendon (2004).

In their study of the monsoon onset during Winter MONEX, Davidson *et al.* (1983) presented evidence that the trigger mechanism for onset lay in the evolution of synoptic-scale weather disturbances to the south and west of Australia. They hypothesized that prior to onset the seasonal buildup of planetary-scale and land-sea temperature gradients reaches a critical stage. Before the onset can take place, however, traveling highs and lows ("weather systems") to the south must be be

configured so that trade easterlies are prevalent across the Australian continent .

The case for triggering of onset by westward propagating, equatorial Rossby waves was made by Hendon *et al.* (1989). As previously mentioned, onset of the monsoon during the 1986/87 season coincided with arrival of the trough of one such Rossby wave (Figs. 8 and 9). Furthermore, another packet of Rossby waves some 3 weeks later also seems to explain revival of the monsoon.

Danielsen (1993) proposed a mechanism whereby the passage of midlatitude cold fronts south of the Australian continent spread cold air northward across the continent, which in turn interacted with the continental scale sea-breeze lying across the northern part of the continent. Such a description bares much similarity to that for the South China Sea cold surges (e.g., Love 1985). Danielsen showed that changes in lower-tropospheric stability and low-level convergence contribute to the triggering of convection and were synchronized with the passages of these higher latitude cold fronts.

Kawamuura *et al.* (2002) propose that onset involves an air-sea feedback, in much the same fashion as discussed by Nicholls (1981), Hendon (2003), and Wang *et al.* (2003) in the context of the SST evolution north of Australia during ENSO. Kwamauura *et al.* suppose that the initial sensible heating of the continent prior to monsoon onset acts to drive shallow north-westerly onshore flow, which superimposes on the mean easterly trades to the north of Australia. Thus, wind speed is reduced, thereby reducing latent heat flux and ocean mixing, hence increasing local SST. Warm SST then promotes stronger north westerly flow (i.e., akin to a Gill (1980) response to an imposed heat source), further reducing the windspeed and warming the SST. Warm SST acts to enhance convective instability , which continues to build up until onset. Onset of the monsoon, in their view, still requires an additional trigger, for instance the passage of the MJO.

5. Modulation of Synoptic Weather

Modulation of synoptic weather (including likelihood of extreme rainfall events) by lower frequency intraseasonal variability is also observed in the monsoon. Enhanced transient kinetic energy at Darwin accompanies the wet phase of the MJO, along with enhanced rainfall variance (Hendon and Liebmann 1990b). The enhanced kinetic energy occurs through the depth of the troposphere but with maxima around 850 hPa and 100 hPa, consistent with the baroclinic structure that is common to many tropical systems. Liebmann *et al.* (1994) also showed a roughly 2:1 modulation of tropical cyclones between wet and dry MJO phases in the Indian and western Pacific sectors (also Hall *et al.* 2001). The hypothesis for such a modulation is that the large-scale MJO anomalies alter the climatologically favourable factors for TC development (e.g. low-level cyclonic vorticity, low vertical wind shear; Gray 1979) on a time-scale that is slow enough that they act in the same way as those climatological base-state factors.

Interestingly, the modulation of TC numbers by low-frequency (relative to the TC) variability is not restricted to the MJO band. A higher and lower frequency bands produce the same degree of modulation. Hence any form of low-frequency (relative to the TC), large-scale variability that alters the dynamical factors favorable for cyclogenesis appears to modulate TC activity.

Wheeler and Hendon (2004) also observed modulation of extreme continental rainfall during the summer monsoon by the MJO. They looked at the contemporaneous relationship between the occurrence of the highest quintile of weekly rainfall across Australia and the phase of the MJO. The normal probability of a weekly rainfall total in DJF being in the upper quintile is, by definition, 20%. Across the Top End region (around Darwin), the probability varies from less than 12% in Phases 1 and 2 (suppressed phase of MJO) to greater than 36% in Phases 5 and 6 (active phase of MJO). This represents more than a tripling of the likelihood of extreme rainfall from the dry to wet phase of the MJO.

6. Interannual Variability and ENSO

ENSO exerts considerable influence on Australian rainfall, but the weakest impact is during the summer season (Fig. 13 from McBride and Nicholls 1983,; see also Holland 1986). Summer monsoon rainfall is modestly correlated with El Niño (~-0.4), but the bulk of this negative correlation comes from a strong negative correlation in the transitional season (Sep-Nov; Table 1 from Nicholls *et al.* 1982). Once the monsoon is active, the correlation of wet season rainfall and ENSO is near zero.

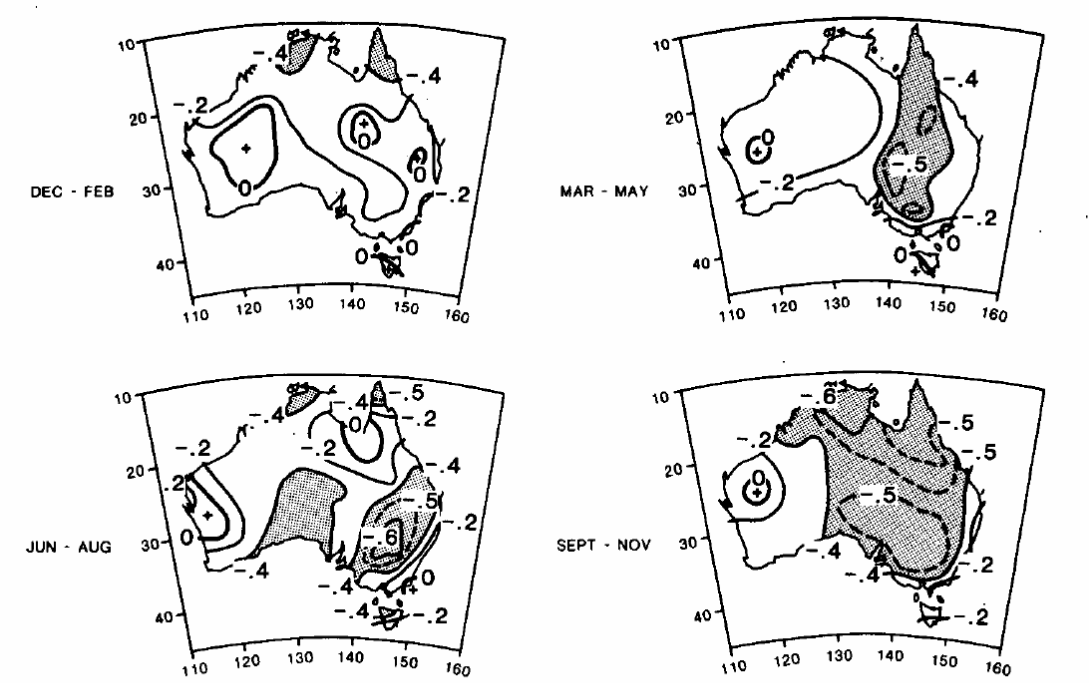

FIG. 2. Simultaneous correlations between Darwin pressure and district rainfall for the four seasons, December–February, March–May, June–August, September–November. Data from 1932–74.

Figure 13 From McBride and Nicholls 1983

Similarly, onset of the summer monsoon, as defined by date of the first 250 mm of rainfall at Darwin, is negatively correlated with El Niño (late onset during warm events, when pressure is high at Darwin; Fig. 14 from Nicholls *et al.* 1982). Because of strong persistence of ENSO anomalies from June through November, onset of the Australian summer monsoon is predictable some months ahead. But, total wet season rainfall is not correlated with onset date (Table 1 from Nicholls *et al.* 1982). Interestingly, onset date as defined by the first 250 mm of rainfall (which is about ¼ of the wet season total) is 3 weeks earlier than onset as determined by the large-scale rearrangement of the tropical circulation. Thus, the strong negative correlation of El Niño with onset date and transitional season rainfall occurs before the summer monsoon circulation is established (i.e., when northern Australia is still in a trade wind regime).

Because of persistence of ENSO anomalies from June-November, onset date of the monsoon is also related to the strength of the previous Indian monsoon (Fig. 15, from Joseph *et al.* 1991). A weak Indian summer monsoon tends to occur during a developing El Niño, which is then followed by a late onset of the Australian summer monsoon. Joseph *et al.* point out that the relationship between the strength of Indian monsoon and onset date of the Australian summer monsoon seems to hold even in the absence of ENSO. They suggest that the Indian summer monsoon is capable of driving SST variations (warm in the western Indian Ocean and cold to the north of Australia), which subsequently act to delay onset of the Australian monsoon. Such possible behavior needs to be explored in coupled

models with ENSO artificially suppressed.

Hung *et al.* (2004) further emphasize that the Australian summer monsoon is not related to the following Indian monsoon, which reflects both the lack of persistence of ENSO after December and lack of simultaneous relationship of the Australian summer monsoon and ENSO. They argue that the Australian summer monsoon acts to disrupt the ENSO cycle.

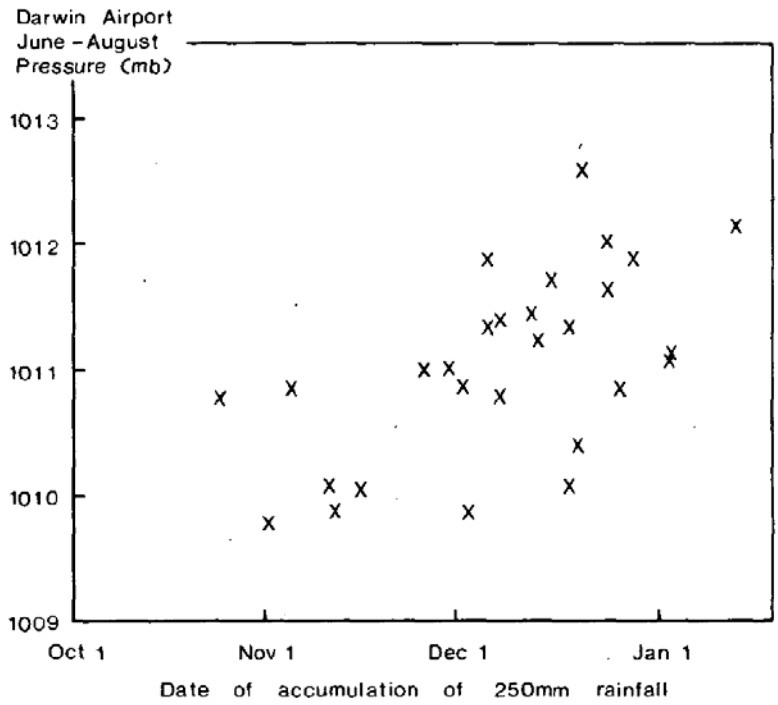

FIG. 2. Scatter diagram of Darwin Airport June–August pressure versus the date by which 250 mm rainfall has accumulated. Data from 1952–80.

Figure 14 Nicholls et al. 1982

Table 1 From Nicholls et al. 1982

TABLE 4. Correlations between the onset indices and Darwin wet-season rainfall. The last row shows correlations between June–August pressure and seasonal rainfall. (The 5% significance level occurs at a correlation of 0.374.)

	Darwin rainfall		
	Sep–May	Sep–Nov	Dec–May
Date of 1st 10 mm	−0.267	−0.477	−0.084
Date of 1st 50 mm	−0.383	−0.707	−0.111
Date of 1st 100 mm	−0.289	−0.817	0.034
Date of 1st 250 mm	−0.394	−0.905	−0.040
Date of 1st 500 mm	−0.520	−0.819	−0.209
Darwin pressure: June–August	−0.335	−0.661	−0.079

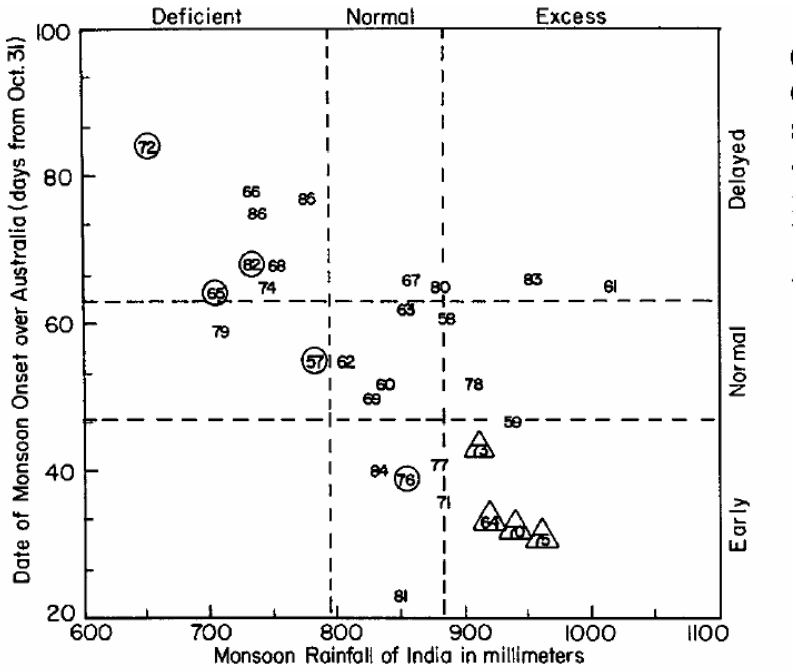

FIG. 2. Scatter diagram between June to September ISMR in millimeters for each of the 30 years 1957–1986 and the date of the following ASMO. ASMO counted as days from 31 October (i.e., 1 November is day 1). Last two digits of year of ISMR mark the location. Each axis is divided into categories of one-half standard deviation and more above the mean, normal, and one-half standard deviation and more below the mean. El Niño years are circled and cold event years are triangled.

Figure 15 From Joseph et al. 1991

Insight into why the ENSO influence on the Australian summer monsoon wanes at the peak of the monsoon is gained by examination of the seasonal evolution of SST anomalies through the ENSO cycle (Fig. 16 from Hendon 2003). In southern winter (JJA) and spring (SON) of an El Niño year, SSTs are cold to the north of Australia and winds are anomalously easterly. These cold SSTs reinforce anomalous subsidence driven by the warm equatorial SSTs in the central and eastern Pacific. Hence, dry conditions in northern and eastern Australia tend to prevail in winter and spring. But, in DJF (summer), despite persistence of warm anomalies in the Pacific and the associated easterly anomalies to the north of Australia, the cold SSTs to the north of Australia disappear. The reinforcement they provide to the remotely forced subsidence thus ends.

The evolution of the SST anomalies to the north of Australia has been postulated to stem from seasonally varying air-sea feedback in the region (Nicholls 1981, Hendon 2003' Wang *et al.* 2003). During the winter (JJA) and spring (SON), the region experiences trade easterlies. In the mean, they act to elevate the thermocline in the eastern equatorial Indian Ocean and to promote upwelling along the Java/Sumatra coast. In other words, in the mean the easterlies produce conditions favorable for air-sea coupling. Anomalous easterlies (for instance, driven remotely by El Niño in the Pacific) at this time of year, then would act to 1) increase the total windspeed (easterly anomaly acting on an easterly

basic state) thereby producing surface cooling through increase latent and sensible heat flux and 2) further elevate the thermocline in the east and promote enhanced upwelling on the Java/Sumatra coast thereby producing more surface cooling in the eastern Indian Ocean. Thus, a positive feedback is produced with colder SST anomalies acting to raise surface pressure in the eastern Indian Ocean and producing stronger easterly anomalies. Once the Australian summer monsoon onsets and the mean winds become westerly, the thermocline in the east deepens and mean upwelling along the Java/Sumatra coast ceases. Anomalous easterlies now acting on a westerly basic state now will decrease the total windspeed, thereby acting to warm the surface. Hence, together with the lack of communication of the subsurface anomalies to the surface (because the mean thermocline is too deep and coastal upwelling is weak), the easterly anomalies will produce a negative feedback. The positive feedback during the winter and spring and negative feedback during summer is offered as an explanation for the strong correlation between onset date and El Niño but for a weakening of the negative correlation between El Niño and northern Australia rainfall once the monsoon onsets.

Other sources of interannual variability of the summer monsoon include seasonal variations of MJO activity. Hendon *et al.* (1999) show years of strong MJO activity tend to occur when convection over Australia is suppressed. That is, years of strong MJO activity tend to be years with a weak summer monsoon. Seasonal MJO activity shows little relationship with ENSO (or any other SST anomalies). Hence, the seasonal rainfall variance accounted for by the level of MJO activity is independent of that accounted by ENSO. However, as the level of MJO activity is not obviously related to SST boundary forcing (Hendon *et al.* 1999, Slingo *et al.* 1999), it is not clear that the MJO-induced component of seasonal monsoon variability will be predictable.

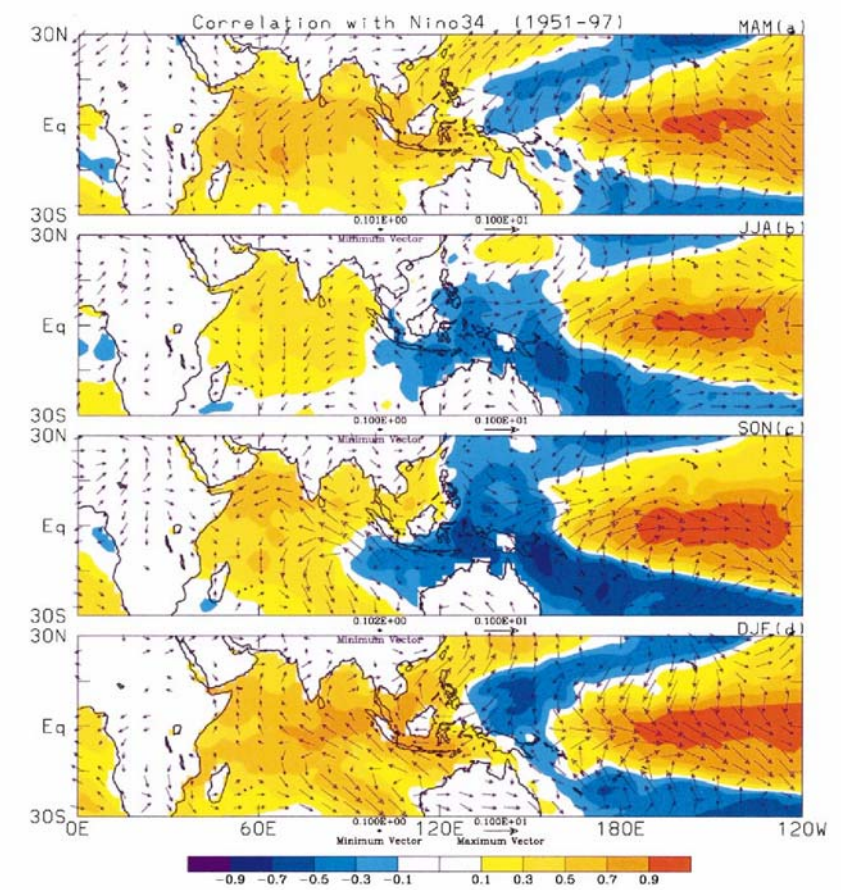

FIG. 5. Seasonal correlation of Niño-3.4 with SST and surface winds for (a) MAM, (b) JJA, (c) SON, and (d) DJF. Plotting convention is same as in Fig. 4.

Figure 16 From Hendon 2003

References

Compo, G.P., G.N. Kiladis, and P.J. Webster, 1999: The horizontal and vertical structure of east Asian winter monsoon pressure surges. *Quart. J. Roy. Meteor. Soc.*, **125**, 29–54.

Danielsen, E.F., 1993: In situ evidence of rapid, vertical irreversible transport of lower tropospheric air into the lower tropical stratosphere by convective cloud turrets and by large-scale upwelling in tropical cyclones. *J. Geophys. Res*., **98**, 8665–8681.

Davidson, N.E., J.L. McBride, and B.J. McAvaney, 1983: The onset of the Australian monsoon during Winter MONEX: Synoptic aspects. *Mon. Wea. Rev*., **111**, 496–516.

Davidson, N.E. and H.H. Hendon, 1989: Downstream development in the Southern Hemisphere monsoon during FGGE/WMONEX. *Mon. Wea. Rev.,* **117**, 1458–1470.

Drosdowsky, W., 1996: Variability of the Australian summer monsoon at Darwin: 1957–1992. *J. Climate*, **9**, 85–96.

Frank, W.M. and J.L. McBride, 1989: The vertical distribution of heating in AMEX and GATE cloud clusters. *J. Atmos. Sci.*, **46**, 3464–3478.

Gill, A.E., 1980: Some simple solution for heat induced tropical circulations. *Quart. J. Roy. Meteor. Soc.,* **106**, 447–462.

Gray, W.M., 1979: Hurricanes: Their formation, structure and likely role in the tropical circulation. *Meteorology Over the Tropical Oceans*. D. B. Shaw (Ed.), *Roy Meteor. Soc*., UK, 155–218.

Hall, J.D., A.J. Matthews, and D.J. Karoly, 2001: The modulation of tropical cyclone activity in the Australian region by the Madden-Julian oscillation. *Mon. Wea. Rev*., **129**, 2970—2982.

Hendon, H.H., 2003: Indonesian rainfall variability: Impacts of ENSO and local air-sea interaction. J. Climate, **16**, 1775-1790.

Hendon, H.H., N.E. Davidson, and B. Gunn, 1989: Australian summer monsoon onset during AMEX 1987. *Mon. Wea. Rev*., **117**, 370–390.

Hendon, H.H. and B. Liebmann, 1990a: A composite study of onset of the Australian summer monsoon. *J. Atmos. Sci*., **47**, 2227–2240.

Hendon, H.H. and B. Liebmann, 1990b: The intraseasonal (30–50 day) oscillation of the Australian summer monsoon. *J. Atmos. Sci*., **47**, 2909–2923.

Hendon, H.H., C. Zhang, and J.D. Glick, 1999: Interannual variation of the Madden-Julian oscillation during Austral Summer. *J. Climate*, **12**, 2538–2550.

Holland, G.J., 1986: Interannual variability of the Australian summer monsoon at Darwin: 1952–82. *Mon. Wea. Rev.,* **114**, 594–604.

Hung, C.-W. and M. Yanai, 2004: Factors contributing to the onset of the Australian summer monsoon. *Quart. J. Roy. Meteor. Soc*., **130**, 739–758.

Hung, C-W., X. Liu, and M. Yanai, 2004: Symmetry and asymmetry of the Asian and Australian summer monsoons. *J. Climate*, **17**, 2413-2426.

Joseph, P.V., B.Liebmann, and H.H.Hendon, 1991: Interannual variability of the Asutralian summer monsoon onset: possible influences of Indian summer monsoon and El Niño. J. Climate, **4**, 529-538.

Kawamura, R., Y. Fukuta, H. Ueda, T. Matsuura, and S. Iizuka, 2002: A mechanism of the onset of the Australian summer monsoon. *J. Geophys. Res*., **107**, No D14, 4204, 10.1029/2001JD001070, 2002.

Keenan, T.D., and L.R. Brody, 1988: Synoptic-scale modulation of convection during the Australian summer monsoon. *Mon. Wea. Rev*., **116**, 71–85.

Keenan, T.D. and R. E. Carbone, 1992: A preliminary morphology of precipitation systems in tropical northern Australia. *Quart. J. Roy. Meteor. Soc*., **118**, 283–326.

Keenan, T.D. and S. A. Rutledge, 1993: Mesoscale characteristics of monsoonal convection and associated stratiform precipitation. *Mon Wea. Rev*., **121**, 352–374.

Liebmann, B., H.H. Hendon, and J.D. Glick, 1994: The relationship between tropical cyclones of the western Pacific and Indian Oceans and the Madden-Julian oscillation. *J. Meteor. Soc. Japan.*, **72**, 401–412.

Love, G., 1985: Cross-equatorial influence of winter hemisphere subtropical cold surges. *Mon. Wea. Rev.,* **113**, 1487–1498.

Matsuno, T., 1966: Quasi-geostrophic motions in the equatorial area. *J. Meteor. Soc. Japan*, 44, 25–43.

McBride, J.L., 1983: Satellite observations of the Southern Hemisphere monsoon during Winter MONEX. *Tellus*, **35A**, 189–197.

McBride, J.L. and W.M. Frank, 1999: Relationships between stability and monsoon convection. *J. Atmos. Sci.,* **56**, 24–36.

McBride, J.L, and N. Nicholls, 1983: Seasonal relationships between Australian rainfall and the Southern Oscillation. Mon. Wea. Rev, **111**, 1998-2004.

McBride, J.L. and T.D. Keenan, 1982: Climatology of tropical cyclone genesis in the Australian region. *J. Climatol.,* **2**, 13–33.

Nicholls, N., 1981: Air-sea interaction and the possibility of long-range weather prediction in the Indonesian Archipelago. *Mon. Wea. Rev*., **109**, 2435–2443.

Nicholls, N., J.L. McBride, and R.J. Ormerod, 1982: On predicting the onset of the Asutralian wet season at Darwin. *Mon.Wea. Rev*., **110**, 14-17.

Slingo, J.M., D.P. Rowell, K.R. Sperber, F. Nortley, 1999: On the predictability of the interannual behaviour of the Madden-Julian oscillation and its relationship with El Nino. *Quart. J. Roy. Meteor. Soc*., **125**, 583–609.

Sumathipala, W.L. and T. Murakami, 1988: Intraseasonal fluctuations in low-level meridional winds over the south China Sea and the western Pacific and monsoonal convection over Indonesia and northern Australia, *Tellus*, A, 40, 205–219.

Troup, A.J., 1961: Variations in upper tropospheric flow associated with the onset of the Australian summer monsoon. *Indian J. Meteor. Geophys*., **12**, 217–230.

Wang, B., R. Wu, and T. Li, 2003: Atmosphere-warm ocean interaction and its impact on Asian-Australian monsoon variation. *J. Climate*, **16**, 1195-1211.

Wheeler , M.C., and J. L. McBride, 2004: Intraseasonal Variability of the Australian-Indonesian Monsoon Region. In Intraseasonal Variability of the Atmosphere-Ocean Climate System, W. K.-M. Lau and D. E. Waliser Eds., Praxis Publishing.

Wheeler, M.C. and H.H. Hendon, 2004: An all-season real-time multivariate MJO index: Development of an index for monitoring and prediction. *Mon. Wea. Rev., (in press for August edition)*.

Wheeler, M., G.N. Kiladis, and P.J. Webster, 2000: Large-scale dynamical fields associated with convectively coupled equatorial waves. *J. Atmos. Sci.*, **57**, 613–640.